UNIVERSITY OF SOUTHAMPTON, 2022

FACULTY OF ENVIRONMENTAL AND LIFE SCIENCES

GEOGRAPHY AND ENVIRONMENTAL SCIENCE

GEOSPATIAL ASSESSMENT OF SOUTHAMPTON ‘GREENER CITY’ PLAN

by

ESER MEHMET KARABOCEK

A dissertation submitted in partial fulfilment of the degree of MSc Applied Geographical Information Systems and Remote Sensing by taught course

September 2022

Student Number: 33037353

Statement of originality

Except for those parts in which it is explicitly stated to the contrary, this thesis is my own work. It has not been submitted for any degree at this or any other academic or professional institution.

Signed

Candidate's name: ESER MEHMET KARABOCEK

ÖZET

Kentsel yeşil alanlar, pek çok şehirde kentin önemli bir bölümünü oluşturmakta ve kentsel alanları birçok yönden etkilemektedir. Yeşil alanların çevresel, sağlık, sosyal ve ekonomik etkileri büyüklük, dağılım ve türlerine göre değişmektedir. Bu nedenle, kentteki yeşil alanların coğrafi/mekansal açıdan değerlendirilmesi büyük önem taşımaktadır.

Bu bağlamda, Southampton, Birleşik Krallık şehrindeki yeşil alanların değerlendirilmesine yönelik bu tez çalışması gerçekleştirilmiştir. 1140 hektarlık açık yeşil alanı ve kentin %18'ini kaplayan ağaç mevcudiyetinin yanı sıra yerleşim bölgelerindeki bahçelerden oluşan özel alanlarıyla şehir, yeşil alandan yoksun değildir.

Çalışmada, şehri içine alan altı adet 5*5 km^2 'lik ulusal grid karelerinin "Environment Agency" tarafından üretilen mevcut yüksek çözünürlüklü görüntüleri ve LiDAR verileri, yeşil alanların türünü belirlemekte kullanılmıştır. Bu amaç doğrultusunda, kontrollü ve kural-bazlı nesne tabanlı görüntü sınıflandırma yaklaşımları uygulanmıştır. En yüksek doğrulukla üretilen "Arazi Örtüsü/Arazi Kullanımı" bilgisi kullanılarak, yeşil alanlar yerleşim yerlerine yakınlığına göre özel ve kamusal olarak sınıflandırılmış ve yükseklik bilgisi kullanılarak ağaçlar tespit edilmiştir.

Çalışma alanının %44.16'sını oluşturan SU31SE gridindeki yeşil alanların %66.8'i ve %51.16'sını oluşturan SU41SW'deki yeşil alanların %68.9'u özel yeşil alanlardır. Ayrıca çalışma alanında kilometrekareye düşen ağaç sayısı 528'tir.

Bu sonuçlar, Southampton'da kamusal yeşil alandan daha fazla özel yeşil alan olduğunu göstermektedir.

ABSTRACT

Urban green spaces constitute a significant part of urban in many cities all around the world and they affect urban areas in many ways. The environmental, health, social and economic effects of the green spaces vary according to the size, distribution, and type of them. For this reason, it is of great importance to assess the green spaces in the city from a geospatial perspective.

In this context, this research project was carried out to green space assessment of Southampton. The city is not a city devoid of green spaces, with its 1140 hectares of open green space and 18% of the city's trees, as well as private green areas consisting of gardens in residential areas.

In this study, the existing data high-resolution images and LiDAR data produced by the Environment Agency of the six 5 km national grid tile covering the city of Southampton were used to identify the type of green spaces. Supervised and rule-based object-based image classification approaches were used to determine green space. Using the LULC information produced with the highest accuracy by these methods, green spaces were classified as private and public depending on the proximity of residential areas trees were detected based on height information.

66.8% of the green areas in the SU31SE 5 km grid, which constitute 44.16% of the study area, are private green areas. 68.9% of the green areas in the SU41SW network, which constitute 51.16% of the study area, are private green areas. In addition, there are 528 trees per square kilometre in the study area.

These results show that there is more private green space than public green space in Southampton.

ACKNOWLEDGEMENTS

First and foremost, I would like to many thanks Dear Dr Gareth Roberts for his guidance and support from the first day of my application process for the master's programme to the submission of this dissertation as programme leader and supervisor of the research project.

Secondly, I would like to thank the academicians who conducted all the modules I completed at University of Southampton. I would like to also thanks my classmates for their friendships.

Sincere thanks to my grandmother, parents and brother for their irreplaceable kindness and moral support whole my life.

Last but not the least, I would like to thank the Turkish Republic for all its financial and moral support throughout this research project and my master's degree.

TABLE OF CONTENTS

LIST OF FIGURES

LIST OF TABLES

ABBREVIATIONS

CASI: Compact Airborne Spectrographic Imager

DEFRA: Department for Environment, Food and Rural Affairs

DEM: Digital Elevation Model

DSM: Digital Surface Model

DTM: Digital Terrain Model

ECW: Enhanced Compressed Wavelet

ESP: Estimation of Scale Parameter

FN: False Negative

FP: False Positive

GB: Great Britain

GIS: Geographical Information Systems

ITCD: Individual Tree Crown Detection and Delineation

LiDAR: Light Detection and Ranging

LULC: Land Use Land Cover

MRS: Multiresolution Segmentation

nDSM: Normalised Digital Surface Model

NDVI: Normalized Difference Vegetation Index

NDWI: Normalized Difference Water Index

NIR: Near Infrared

NN: Nearest Neighbour

OBIA: Object-Based Image Analysis

OBIC: Object-Based Image Classification

OS: Ordnance Survey

OSGB: Ordnance Survey Great Britain

OSM: Open Street Map

RADAR: Radio Detection and Ranging

SP: Scale Parameter

TN: True Negative

TP: True Positive

UGS: Urban Green Space

UHI: Urban Heat Island

UK: United Kingdom

VHR: Very High-resolution

WHO: World Health Organization

1. INTRODUCTION

1.1. Urban Green Space

There is no sole definition of green space globally accepted and used by authorities. Green space is defined depending on disciplines and qualitative or quantitative criteria (Taylor and Hochuli, 2017). However, in its most comprehensive expression, it can be defined as a range of vegetation (Almanza et al., 2012).

Green spaces are expressed in various terms such as forest, park, and grassland according to their geographical location and usage purposes. Urban green space (UGS), the research area of this study, is one of the most widely used terms to express green areas.

Boulton et al. (2018) defined UGS as only non-privately owned vegetated areas in urban. Moreover, the European Commission (2012) defined UGS, one of the European urban atlas classes, as space consisting only of forests, open green spaces mainly used for recreational purposes and suburban parks. Moreover, a significant portion of the tree presence in urban areas is found in the parks (Shanahan et al., 2015). Also, street trees are an essential part of UGS, especially in well-planned cities (Wood and Esaian, 2020).

However, green spaces in the city do not only consist of public open properties. Domestic private green areas around dwellings, which are part of cities, usually called private gardens, are also part of the UGS. In addition, UGS are defined by land characteristics as well, independent of if they are private or public (Zou and Wang, 2021).

The main reason UGS is a concept defined in many ways is that it is one of the joint study subjects of different disciplines. To date, there are many studies on green spaces in cities. However, the definitions of public and private green spaces and their differences from each other, and especially the issue of whether private green areas can be considered a part of the UGS, are still unclear. Arguments still to be clarified about UGS like this may be among the new and highly preferred topics of UGS studies in recent future.

On the other hand, the contribution of public green space to the liveability of the living environment and the experience of nature are crucial elements. One distinguishing element of the domestic garden is that it is regarded as an outside living space that provides casual recreation. Consequently, public and private green spaces are not interchangeable features (Coolen and Meesters, 2012). This means UGS are composed of elements that differ from each other. However, to reveal this variation, it is necessary to map the green areas in the city primarily.

The speed of developments in geospatial technology has added a new dimension to this issue. These developments have contributed to local, national, and global decision-making authorities such as city councils, ministries, and international organizations to take action to ensure the sustainability of urban green spaces that fall under their responsibility. In this context, many institutions publish various plans and reports for the present and future of green spaces in their cities. For instance, United Nations (2015) has set the goal of building greener and more accessible green spaces to make cities resilient within the framework of sustainable development goals. The European Commission (2013) has adopted the strategy of protecting and developing green areas.

In addition, local authorities carry out a series of studies for the planning and continuity of UGS. "Southampton City Council Green City Plan 2030" prepared by Southampton City Council is one of them.

1.2. Southampton Council Green Space Policy

Southampton, with an estimated 267,000 single trees covering 18% of the city and a population of 262,000, has trees one per capita. Besides, it is rich in public green space with 49 parks and 1,140 hectares of open green space (Southampton City Council, 2020). In addition, with an average garden size of 152 m^2, it is above the UK average of 130 m^2 (ConservatoryLand, 2021). Nevertheless, these values alone are not an indication of whether the green areas in the city are sustainable, healthy, and capable of adding economic and social added value to the city. Many different parameters such as the location, spatial distribution, accessibility, phenological and biochemical characteristics of UGS affect the quality and sustainability of a city.

The necessity of cities to be greener and thus environmentally sustainable places for the life of living things has made it inevitable to take actions proactively against climate change as soon as possible. In line with this purpose, many different authorities have published plans stating when and how they will act on this issue. In this context, Southampton City Council has also published a plan "Southampton City Council Greener City Plan 2030" in 2020.

Within the framework of this plan published to raise Southampton to higher standards in different aspects for today and future generations, it aims to make the city a greener, healthier, cleaner, and sustainable city identity, and how these goals would be achieved was explained in detail. Therefore, to achieve these ultimate purposes, the policy of increasing green spaces in the city and making them better quality areas has been shaped in line with the objectives of the city's themes of clean air, health and wellbeing, clean and environmentally friendly transportation, and carbon reduction (Southampton City Council, 2020).

1.3. Aims and Objectives

The overall aim of this research project is to assess green spaces in Southampton geospatially by producing visual and numerical outcomes as maps and charts to show the distribution of private and public green spaces and tree density using high spatial resolution aerial images and LiDAR data provided by Environmental Agency of the Department for Environment, Food and Rural Affairs (DEFRA).

To achieve the overall aim, these objectives determined:

- To produce a land use/land cover information of the study area using the Object-based image classification technique
- To separation of public and private green areas in the study area with spatial approach

2. LITERATURE REVIEW

This section aims to evaluate the effects of urban green spaces and the approaches used in the spatial analysis of these areas by bringing a critical perspective to the literature produced so far. In section 2.1, the effects of urban green areas will be examined in environmental, health and economic and social aspects by introducing relationships of spatial evaluation of urban vegetation with these aspects. In Section 2.2, current methods and data used in the literature to perform the identification, mapping, and spatial assessment of UGS will be critically analysed. Classification methods used in UGS studies will be discussed in Section 2.3. Finally, it will reveal how the gap in the literature about separating UGS as public and private can be filled with available data of the study area.

2.1. Effects of Urban Green Space

UGS has the capacity to affect the world in many ways, both with its content and depending on its location. UGS can provide various benefits and cause some threats to living and non-living creatures around them, mainly due to their location and spatial distribution (Bradley and Altizer, 2007; Roy et al., 2012; Shackleton et al., 2015).

2.1.1. Environmental Effects

Since the beginning of the 20th century, as urbanisation is growing rapidly than ever before most places on the world, the effects of green spaces in cities have started to be discussed (Clark et al., 2017). With the increase in the population living in the city, the size of the cities expands, and the need to offer new living spaces, transportation facilities and various job opportunities to new citizens in the cities arises (Dieleman and Wegener, 2004; Nissar and Nuzhat, 2016; Zhao et al., 2010). All these developments contribute to human civilisation (Lim and Lee, 2012; Plaziak and Szymanska, 2014; Schumacher and Duan, 2020). However, there are plenty of drawbacks to the consequences of urbanisation. It is estimated that the decrease in green areas caused by the expansion of cities will not only be limited to in city itself but will also cause a decrease in green arable land (Tan et al., 2005). Bren d'Amour et al. (2017) have stated that the expansion of urban areas will cause around 2 per cent of cropland in the world will be lost in 10 years. Outcomes of urban expansion and eventually loss of green space cause various damages to cities in terms of the environment, such as the increase in urban temperature, decrease in air quality, and reduction in biological diversity (Bilgili and Gökyer, 2012).

The underlying reasons for the reduction of UGS fields both human related and originating from nature. Natural disasters such as erosion, flood and drought also cause a severe reduction of green areas in cities (Yang et al., 2019). Minimising the negative impacts of natural disasters in cities is directly related to the increase in the presence of green zones, and natural disasters threaten the continuity of green areas (Chunyan et al., 2016). On the other hand, green areas diminish or even eliminate the destruction caused by disasters (Jeong and Yoon, 2018). Kim et al. (2016) suggested allocating resources for developing green spaces in cities and that these efforts should identify the ideal locations to establish UGS to prevent flood damage.

Provided that the green areas in the city are well protected, they significantly contribute to biodiversity. At a first glance, although it is thought that urbanisation will lead to a decrease in green land in that region and negatively affect biodiversity, a well-maintained green area continues to contribute to the continuity of fauna and flora in that region (Goddard et al., 2010).

For example, in Sheffield, private green spaces in urban are home to more plant and animal species than rural green spaces (Gaston et al., 2005). Moreover, public UGS, particularly semi-natural and human-made green areas, such as city parks, can offer new living spaces to living things because of their different soil structures from the surrounding areas. These places offer living things a unique habitat opportunity. For instance, there is not much difference between tropical forests, arctic tundra with no urbanisation and the Central Park in downtown New York in terms of underground biodiversity (Ramirez et al., 2014).

However, the lack of UGS causes serious problems. There is an anthropogenic temperature rise with heat flow from buildings, people, and trees toward the city, especially in areas where built-up are concentrated (Bassett et al., 2016). For instance, urban areas in the UK are up to 7 °C hotter than the nearby countryside (Wilby, 2003).

In addition, the evolution of impermeable areas from vegetation or plains has led to the formation of harmful environmental circumstances such as urban heat islands (UHI) (Xu et al., 2009). UHI is a representative occurrence of urban climate change according to numerical indicators, defined as an increase in air temperature, especially in certain parts of cities. The UHI effect is one of the leading causes of the global climate change problem

(Masson et al., 2020; Santamouris, 2018). Nonetheless, UGS decreases the heat storage in cities compared to concrete structures because vegetation boosts urban albedo, and vegetated areas have a lower temperature than artificial features with the same albedo (Shashua-Bar and Hoffman, 2000). Therefore, increasing the amount of grassland in urban areas can significantly contribute to lowering the UHI (Armson et al., 2012).

Besides that, UGS contribute a great advance to the prevention of air and water pollution. Air pollution in urban areas is up to 25 times higher than in nearby rural districts (Heidt and Neef, 2008). Nonetheless, green areas create less gas emissions compared to built-up areas, positively affecting the city's air quality (Semeraro et al., 2021). UGS may significantly contribute to a city's infrastructure by enhancing water quality and mitigating runoff (Zhang et al., 2012). Mukherjee and Takara (2018) stated that urban water is improved in both quality and quantity by green space by retaining runoff and increasing ground recovery. However, all these environmental benefits of UGS are possible when they are in the right location and when its spatial expansion is planned.

2.1.2. Health Effects

Although the positive effect of the presence of green space on human health is a phenomenon known throughout history, the reasons behind this situation were not sufficiently understood until the 2000s. They could not be revealed meaningfully due to insufficient scientific evidence and method (WHO, 2016).

Green spaces have a variety of benefits for both physical and mental health (Ridgley et al., 2020). Open green spaces contribute to people's well-being by providing a location for city residents to rest, interact socially, and engage in physical activity (Shanahan et al., 2015). Gascon et al. (2016) estimated a negative correlation between green space amount and the risk of death from heart disease. Due to the opportunities offered by public parks for physical activity, public green spaces positively contribute to the prevention of obesity (Lachowycz and Jones, 2011). In addition, Twohig-Bennett and Jones (2018) stated that the blood pressure and cholesterol values of people with more green areas around and exposed are healthier.

Furthermore, UGS also has a positive effect on people's mental health. Andrusaityte et al. (2020) found that each hour spent by children aged 4-6 in parks reduces their risk of experiencing mental problems. Green spaces also have a positive effect on the mental health of adults. Astell-Burt and Feng (2019) stated that when people spend time in areas with dense trees and grass, it reduces the likelihood of experiencing psychological problems.

Private gardens also contribute to human health, especially mentally (Dennis and James, 2017; Soga et al., 2017). The inability to go to open spaces due to the conditions created by COVID-19 has increased the impact of private gardens on human health (Lehberger et al., 2021). Spending time in their domestic gardens during lockdowns implemented to prevent the spread of the COVID-19 pandemic has increased their physical and well-being and reduced the anxiety caused by the pandemic (Corley et al., 2021; Theodorou et al., 2021). Darcy et al. (2022) stated that during the first national lockdown in the UK (23 March–18 June 2020) after the Covid-19 pandemic emerged in the UK, spending time in a private garden while people must spend time at home benefits physical and cognitive health.

However, contrary to all these positive contributions of green space in cities to the health of humans and other living things, some aspects can cause serious health problems. For example, pollen and epidemic-causing microbes can spread quickly in and around green areas, primarily through flying creatures. As a result, diseases spread from vegetation to urban living areas and can reach a situation that can harm considerable populations. To take proactive measures before severe health risks, which can threaten human life, occur, the locations, distribution and contents of green areas must be determined meticulously, and their persistence must be ensured (Lõhmus and Balbus, 2015). In addition, Collins et al. (2020) suggested that a measure of green space quality should be established using existing geospatial data to reveal the relationship between green spaces and mental health more clearly. Therefore, how green spaces are located and distributed within the city is vital for a healthier society.

With the new methods developed and the ease of access to data on health and green spaces, the scientific reasons for the positive effects of UGS to human health as well as, it will enable more than today further research on the relationship between green space and non-communicable diseases such as mental illness, stroke, obesity, type 2 diabetes, heart diseases and cancer caused by stress load and lack of physical activity in many cases. These diseases negatively affect physical and mental health and influence individuals and states economically and socially. Experienced health problems and treatment processes cause individuals to avoid labour force activities, thus reducing employment and production. It also imposes an economic burden on them and causes an increase in government health costs (Shortt et al., 2014).

2.1.3. Economic and Social Effects

Cities have become more attractive places for many people than the countryside. Today, the number of people in cities is higher than ever before and it is thought that the tendency to live in cities will continue in the future (United Nations, 2019). As of 2020, only 17.1% of the population in the UK lives in rural areas, while the proportion of the population living in cities is 82.9% (DEFRA, 2021). The economic and social opportunities offered by the city are the main reasons for the migration of people from villages to cities. Ahern (2011) has claimed that by the middle of the current century, seven out of ten people will live in urban areas worldwide. Although this trend has led to discussions about whether many opportunities for city life will be sustainable in the future, people's demand for green space will continue. In this respect, access to open green spaces and having a private garden are critical socioeconomic aspects, particularly in city life (Coolen and Meesters, 2012). However, not everyone has a privately owned green area. For example, 12% of households do not have their own green space of their own in Great Britain, and the shortage is more prevalent in some sociocultural and economic classes than in others (Office for National Statistics, 2020).

Even if some green spaces outside the city have the same or similar physical characteristics as urban living spaces, they cannot provide the social benefits of urban green spaces. Having easily accessible green spaces in the city offers unique opportunities for people to socialize and spend quality time (Havinga et al., 2020). Making the spatial evaluation of UGS will positively contribute to the individuals who make up the society to gain the habit of living together and mitigate the destructive effect of socioeconomic gaps (Hoffimann et al., 2017). For this reason, it is significant where the public UGS will be located, their proximity to dwellings, their accessibility, their number, and how their spatial distribution will be. The fact that these parameters can provide the most benefit for the most people can be possible by geospatial attachment of urban green areas from a multifaceted perspective. However, more research are needed to compare the socioeconomic consequences of the spatial relationships between open public green spaces and private gardens in cities.

To present dissimilarities between these two green space types more clearly, UGS need to be assessed in terms of their social and economic effects.

2.2. Mapping Urban Green Spaces

Many approaches have been tried, developed, and employed to obtain information about urban green spaces. Initially, from the 1970s to 2000, manual digitization of printed maps and aerial photographs was the primary method to extract and interpret information for UGS research (Jim,1989; Nowak et al., 1996; Spronken-Smith and Oke, 1998). In the following years, with the increase in data accessibility and diversity, and more importantly, the cost-effectiveness of digital image processing techniques that enable such data, manual methods have been displaced by remote sensing science in UGS studies (Pu and Landry, 2012).

The development of remote sensing technologies has allowed it to obtain high-resolution data for free. In this way, remote sensing has a remarkable place in city studies on green spaces (Rosina and Kopecká, 2016). Almost all studies on UGS require remotely sensed geospatial data and processing methods to conduct their research. However, some studies continue to use field research techniques on specific issues related to UGS (Hettiarachchi and Wijesundara, 2017; Moon et al., 2018; Szilassi et al., 2020). At the same time, high-resolution remotely sensed data has become more available. Therefore, the number of UGS studies in which only remotely sensed data has been used as a source has significantly increased last twenty years (Shahtahmassebi et al., 2021). Accordingly, remotely sensed data has become the primary data source of UGS studies (Chen et al., 2018). Because of this development, the data obtained from field surveys for UGS studies has largely been replaced by very high-resolution (VHR) remote sensing images (Huerta et al., 2021).

The data sources in UGS studies are not only VHR images. Medium resolution satellite images have been used in many UGS studies. For example, Yu et al. (2017) used 30-m spatial resolution Landsat 5-TM and Landsat-8 OLI for UGS classification to calculate cover fraction of vegetations and Jensen et al. (2004) used ASTER image to show the relationship between urban forests and quality of life.

On the other hand, VHR data has become the most common source in UGS studies. For example, Quckbird images have been used to map UGS in several studies (Lang et al.,2008; Van de Voorde, 2017). Asmaryan et al. (2013) used approximately 2 m spatial resolution WorldView-2 data to map street trees cause urban pollution and Nouri et al. (2018) used WorldView-3 data to produce soil salinity map of UGS. In addition to that, aerial photographs also one of the main sources in UGS studies and have been used for various purposes, such as to measure of tree density in the city with calculation Normalized Difference Vegetation Index (NDVI) and evaluating of green quantity in urban areas (Franco and Macdonald, 2018; Liang et al., 2017).

In addition, active remotely sensed data are also preferred for UGS studies, particularly airborne LiDAR technique is one of the common data sources in UGS mapping studies with the advantage of ability of producing height information of vegetation (Caynes et al., 2016). LiDAR sensors can generate precise information on the vertical composition of vegetation within UGS using pulse with wavelength. While LiDAR data used as an only data for some UGS mapping studies, such as for mapping trees on the wayside (Tanhuanpää et al., 2014) and habitat suitability for vegetation (Cheng et al., 2017), some studies were conducted by using combination LiDAR with high-resolution images, such as estimation of tree canopy cover (Parmehr et al., 2016) and tree species detection (Tigges et al., 2013).

All these studies, which are carried out using different data types and techniques, are almost entirely only about public open green spaces. However, private green spaces constitute a considerable part of UGS in many countries (Goddard et al., 2010). Although domestic gardens are the most significant part of UGS in the UK, there are very few studies on private green spaces about the UK (Mathieu et al., 2007).

Gaston et al. (2005) conducted one of these studies to analyse the geometric, volume and associated attributes of private gardens in Sheffield, UK. They used two different approaches for this purpose. Firstly, dwellings were selected randomly from Sheffield digital maps, and private gardens were determined by using grid references of the midpoints of these dwellings. Subsequently, they defined it as dwellings and private gardens belonging to the dwelling through quadrat areas of 100 m. However, Gaston et al. (2005) stated that both approaches are insufficient to distinguish whether the type of use of the areas is private or not and cannot separate the pavements, other concreted areas or temporary sheds, greenhouses, and similar structures from the private garden. Therefore, the geospatial and content properties of the private green spaces in the city could be determined, through information obtained by telephone survey. There are also studies that identify private green spaces only using remotely sensed data. For example, Mathieu et al. (2007) calculated the distribution of the private garden in the study area using the object-based classification technique. After classification using IKONOS satellite images, the UGS in the residential area were visually classified according to the vegetation content. Then, training samples from these classes were selected and the distribution of private UGS was calculated with the supervised object-based image analysis (OBIA) approach. However, the approach chosen by Mathieu et al. (2007) was based on visual interpretation relying on their experience although the detection of private UGS was determined by its spatial relation to residential areas. In addition, quantitative geospatial analysis did not use for private UGS detection. Nevertheless, the approach has the advantage of high accuracy and speed.

2.3. Image Classification in Urban Green space Studies

Classification approach is one of the most preferred methods in UGS studies (Shahtahmassebi et al., 2021). LULC classification for the detection of green areas in cities is carried out by pixel-based or object-based classification methods (Kwan et al., 2020).

2.3.1. Pixel-Based Classification in Urban Green Space Studies

Traditional pixel-based classification algorithms are insufficient for acquiring information about urban vegetation because of the high spectral diversity in the cities (Shojanoori and Shafri, 2016). However, the pixel-based classification technique has been used in some studies on UGS. For instance, Liu and Yang (2013) extracted vegetation cover in the urban area successfully using a supervised pixel-based classification technique.

On the other hand, the results can be lower accurate in UGS studies with pixel-based classification. Taubenböck et al. (2012) misclassified some small gardens as residential areas, result of pixel-based classification using RADAR data.

OBIA approach outperforms pixel-based classification in terms of detecting grassland, urban forests, and tree species because it combines shape, colour and spatial feature information to segment pixels and classify objects (Li et al., 2010). Shackelford and Davis (2003) tested whether the pixel-based or object-based classification technique outperforms the classification of urban using high-resolution IKONOS images. They found that the object-based classification of trees and grasslands was approximately 11% more accurate than pixel-based classification.

2.3.2. Object-Based Image Analysis in Urban Green Space Studies

The OBIA method has been used in many UGS studies. The OBIA approach allows for the extraction of comprehensive data about various objects in urban due to its capacity to use high-resolution data effectively (Gülçin and AKPINAR, 2018).

The data sources in OBIA method are mainly unmanned aerial vehicle images, airborne LiDAR, and image data WorldView-2, GeoEye, QuckBird and IKONOS satellite images (Ma et al., 2017b). However, the number of UGS studies which used spatial resolution of less than 1 m is very limited (Vigneshwaran and Vasantha, 2021).

The OBIA method was preferred for many different studies, such as green mapping of the city (Shekar and Aryal, 2019), index development for UGS quality (ThiLoi et al., 2015), urban green volume calculation (Huang et al., 2013). Consequently, OBIA has become a common approach, replacing the traditional pixel-based classification method (Blaschke et al., 2014).

2.4. Summary of Literature Review

Although many techniques and data sources are used to map UGS, there is less research in some study fields. The number of studies on the distribution of trees in the city and the public and private green space are very few compared to other subjects. Especially although private gardens are represented by a significant number of pixels in VHR images, is one of the compelling reasons that only a few studies have been done so far in this research area (Mathieu et al., 2007).

Urban green spaces must be sustainable together with the cities they are a part of for their advantageous effects on their environment to continue and function effectively. However, this can only be possible with more and better studies in these areas, an issue where many different fields of study intersect. To create more liveable urban living spaces, identifying green spaces in the city and identifying these areas in terms of open or private has a vital role in ensuring the effective management and sustainability of UGS.

There are many studies in the literature on UGS. Various data sources and techniques have been applied in these studies. In general, it can be said that higher accuracy results will be obtained when using remotely sensed data with higher spatial resolution. There is a trend of using the OBIA method rather than the pixel-based approach in the classification studies.

Many UGS classification studies have been carried out using the OBIA method. Both techniques have advantages and disadvantages compared to each other. However, for urban mapping research using high-resolution imagery, the object-based classification system is better than the conventional per-pixel classification methods.

In UGS studies where remote sensing technique is used, UGS mapping studies are mostly encountered. The subject of mapping of green spaces in urban areas is more common than species mapping, biomass and carbon studies and change detection analyses in which UGS are selected as the subject of study. Although there are many studies in the field of UGS mapping, there are very few studies on private gardens, which are a critical part of the urban ecosystem. Therefore, more studies on private gardens are needed.

Within the scope of this research project, it has been decided that using the OBIA approach with the LiDAR-derived DEM and vertical aerial photographs belonging to the city of Southampton is the most appropriate materials and method following the purpose of the research project.

3. METHODOLOGY

This chapter aims to describe the approach used in this project. In section 3.1 the methodology will be introduced with the main lines. In section 3.2 and 3.3 the study area and dataset will be explained, respectively. In the following sections of the chapter, it will be described how the results are produced by using which approach for the study area and how the validation of these results is carried out.

3.1.Overview

The workflow of the project is shown as a flowchart in Figure 3.1.

Throughout the study, three different software were used for various purposes. The pre-processing required for the downloaded data to be suitable for object-based classification was carried out in ENVI 5.6 and ArcGIS software. The classifications were made using eCognition Developer 9. The accuracy analyses of the classifications, mapping the distribution of trees and determining and visualising the distribution of public and private green spaces in the study area was carried out using ArcGIS Pro.

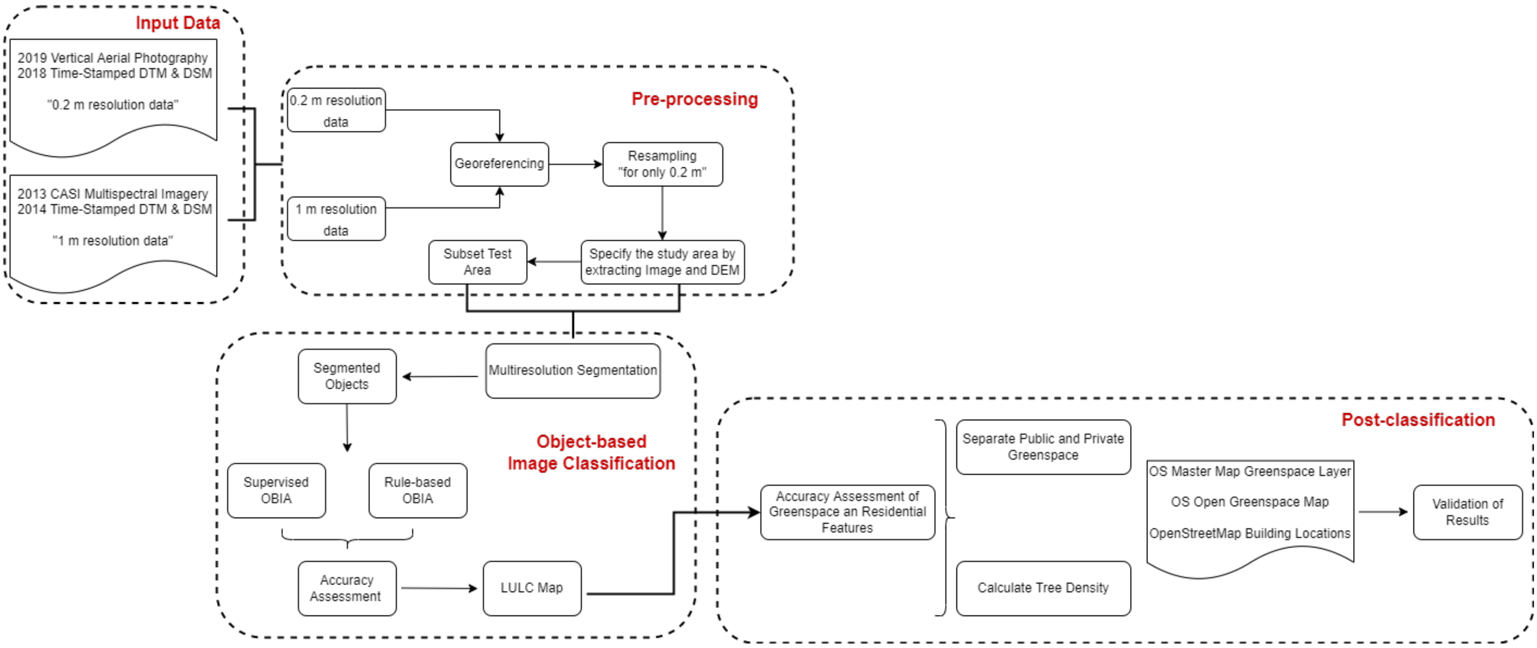

Figure 3.1 Overall flowchart of the study

3.2.Study Area

Initially, the study area was first selected as six five-by-five km national grid tiles (Figure 3.2), which covers the area of the city of Southampton. These grid tiles are SU31NE, SU31SE, SU41NW, SU41SW, SU41NE and SU41SE. The available data (Table 3.2) in these tiles were downloaded from the Department for Environment Food & Rural Affairs (DEFRA) survey data download website (https://environment.data.gov.uk/DefraDataDownload/?Mode=survey).

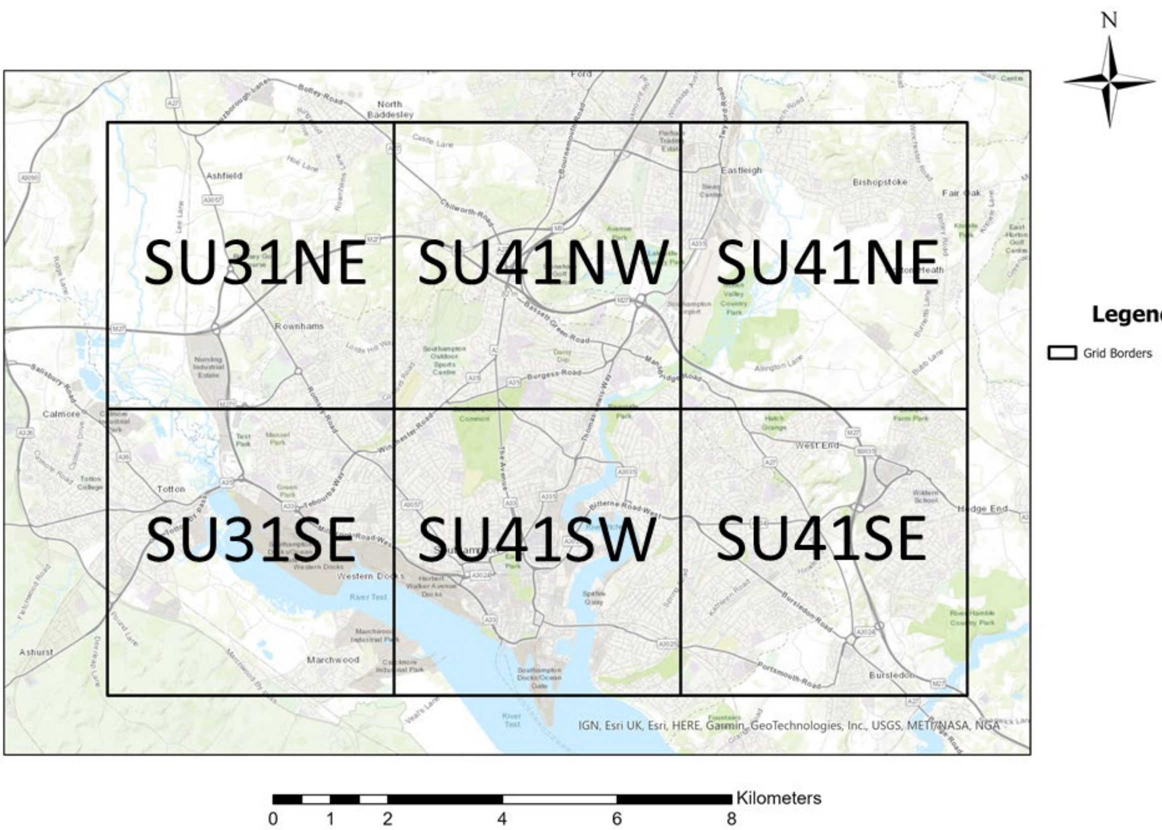

Figure 3.2 The 5 km Grid Tiles

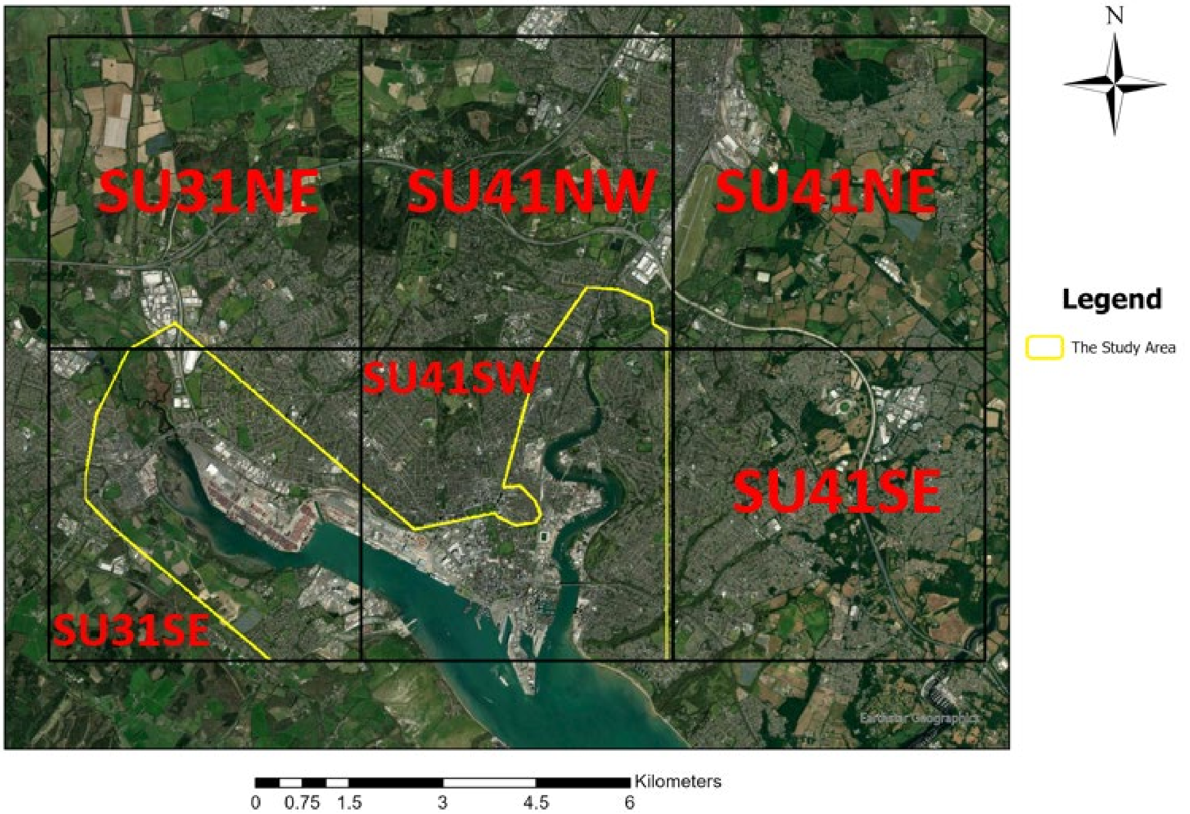

Figure 3.3 The study area

Thereafter, the study area was decided as overlap area (Figure 3.3) of mosaicked available the recent datasets, which are 2019 vertical aerial photographs and 2018 Time-Stamped DSM and DTM. The study area of this project is approximately 34.07 km^2 and consists of various urban features such as docks, residential buildings, industrial areas, public and private green spaces, water, railway, highway, parking lots.

Table 3.1 Grid tiles of the study area consists

Tile Name	Percentage of the Study Area
SU31NE	0.71
SU31SE	44.16
SU41SW	51.16
SU41NW	3.97

The study area, which is formed after the data is obtained and pre-processed, contains data of four different grid tiles. Table 3.1 indicates what percentage of the study area is at which grid tile.

3.3.Dataset

The input data of this research project consists of high spatial aerial images and DSM and DTM data derived from LiDAR data (Table 3.2). Also, for the validation of the analyses, vector data were used which are, Ordnance Survey (OS) Open Green space, OS Master Map-Green space Layer, building locations from OpenStreetMap (OSM) (Table 3.6).

Table 3.2 Input datasets of the project

Data		Format & Resolution	Year	Source
Aerial Images	Vertical Aerial Photographs	ECW Format – Raster 20 cm spatial resolution 8-bit unsigned	2019	The Environment Agency
	CASI Multispectral Imageries	GeoTIFF Format – Raster 1 m spatial resolution 16-bit unsigned	2013	
Airborne LiDAR Digital Elevation Models (DEM)	Time-Stamped Digital Surface Model (DSM)	GeoTIFF Format – Raster 1 m spatial resolution 32-bit float	2014 & 2018	
	Time-Stamped Digital Terrain Model (DTM)			

Data are shown in Table 3.2 were downloaded as separate ZIP files for each of the five-by-five km national grids that cover the study area.

In post-classification analyses, the data shown in Table 3.6 were used to validate the outputs produced as a result of processing the input data.

3.3.1. Aerial Images

The latest produced one among the input datasets are vertical aerial photographs. The images were acquired via a high-resolution camera positioned under the aircraft to obtain reflectance data in the red, green, blue and near infra-red spectrum on 22/08/2019. The dataset consists of orthorectified, using simultaneous GPS and LiDAR data, vertical aerial photographs in ECW (Enhanced Compression Wavelet) format 20 cm spatial resolution as four spectral bands, NIR bandwidth is 780-880 nm, each corresponding to OS one-by-one km grid tile (Environment Agency, n.d.). These data consist of 67 files in total (Table 3.3).

Table 3.3 Number of files of vertical aerial imageries based on the tiles

Ordnance Survey 5 by 5 km Tile Name	**Number of ECW Files**
SU31NE	2
SU31SE	21
SU41NE	1
SU41NW	3
SU41SE	19
SU41SW	21
Total Number of Files	67

Another high spatial resolution data used in the study are the images captured on 09/07/2013 with CASI (Compact Airborne Spectrographic Imager) 1500 push broom sensor. These are in GeoTIFF format with 1 m spatial resolution consisting of 22 spectral bands (Table 3.4) and projected based on the British National Grid coordinate system. Each file contains mosaiced images covering five-by-five km tiles. That is, data of each tile is available as single raster data. Besides this raster data, vector data in shapefile format that cover the same area is also available in the same file.

Table 3.4 CASI Multispectral Imagery Bands

Band Number	Waveband Centres (nanometres)	Spectral Region
1	394.3	
2	442.0	
3	487.3	BLUE
4	512.4	
5	555.2	GREEN
6	576.7	
7	596.9	
8	611.2	
9	624.3	
10	642.2	
11	662.4	RED
12	674.3	
13	685.0	
14	692.2	
15	701.7	
16	711.2	
17	748.1	
18	799.3	
19	854.1	
20	879.1	Near Infrared
21	959.0	
22	1007.9	

3.3.2. Digital Elevation Models

DSM and DTM data were used to get the height information. While selecting the most pertinent DEM data for the project, the footprints of the DEM were checked, starting with the data produced most recently to aerial images. Attention was paid to selecting the DEM data, which contained the much available data and was produced close date with aerial images and has a common footprint. Consequently, 2018 time-stamped DTM and DSM data were selected for use with the 0.2 m spatial resolution 2019 vertical aerial photographs, and 2014 time-stamped DTM data for use with the 1 m spatial resolution 2013 CASI multispectral image.

DEM datasets of 2018 and 2014 consist of single band raster models with 1-meter spatial resolution derived from point clouds obtained by the airborne LiDAR surveying technique performed by Environmental Agency teams between October of the previous year and April of that year. These are in GeoTIFF format and have +/- 15 cm root-mean-square error. The data of the five-by-five km grid tiles consists of ZIP files containing the data of not only one-by-one km OS grid tiles like vertical aerial photography but also two-by-two grid as well. However, all DEM in five km grid tiles files have 1-meter spatial resolution regardless of the size of tiles.

The DEM data (2018) used in this study are the DSM and DTM data produced using the point cloud data obtained by airborne LiDAR technique with the flights carried out on the 1st and 2nd of February 2018. These data were produced on 12/04/2018 and made available on 04/12/2019. Also, the DEM data (2014) obtained with same procedure flights on 29/03/2014 and 31/03/2014. The data produced on 08/04/2014 and made available 04/12/2019. The number of files of DEM data is shown in Table 3.5 for each 5 km grid tiles.

Table 3.5 Number of DEM files used in this study

DEMs – 2014			**DEMs – 2018**		
Ordnance Survey 5 by 5 km Tile Name	**Number of TIFF Files**		**Ordnance Survey 5 by 5 km Tile Name**	**Number of TIFF Files**	
	DSM	**DTM**		**DSM**	**DTM**
SU31NE	10	5	SU31NE	5	5
SU31SE	16	8	SU31SE	8	8
SU41NE	4	2	SU41NE	2	2
SU41NW	7	4	SU41NW	4	4
SU41SE	8	4	SU41SE	3	3
SU41SW	16	8	SU41SW	8	8
Total Number of Files	92		**Total Number of Files**	60	

3.3.3. Reference Data

Vector data in shapefile format produced by OS were used to determine the accuracy rates of the results of classification of the input data. One of the reference data is OS MasterMap Green Space-Layer data. The dataset was produced on 21/09/2021. The current version used in this study is October 2021 version. This data is on a scale of 1:2500, each corresponding to a five-by-five km grid size. Locations of all public and private green spaces in the study area are available in the dataset. In this study, the data was used for private green space validation. The other data is OS Open Greenspace vector data. The latest available version of this data, updated in April 2022, was used in this study. This 1:25000 scale data includes open/public green spaces in the city. For building location weekly updated OpenStreetMap Planet.osm building layer were downloaded from bbbike.org. GB National Grid Squares data comprised by 1, 5, 10, 20, 50 and 100 km national grid squares layers in British National Grid coordinate system. In the scope of this research, 5 and 1 km grid tiles were used.

Table 3.6 Reference data used in the study

Data	Purpose of Use for this Study	Format & Resolution	Year	Source
OS Master Map Greenspace – Layer	Private Green spaces	1:2 500 Shapefile – Vector	October 2021	Ordnance Survey
OS Open GreenSpaces Map	Public/Open Green space	1:25 000 Shapefile – Vector	April 2022	
OS GB National Grid Squares	Grid Border	1:250 000 Shapefile – Vector	December 2012	
OpenStreetMap Planet.osm	Building Locations	Vector	August 2022	Planet OSM

3.4. Data Pre-Processing

As a first step, one-by-one km grid DSMs and DTMs were mosaicked separately to acquire five-by-five km grid DEM data. Then, these mosaicked DEM of five km tiles data were mosaicked and exported to acquire DSMs and DTMs of the study area. This process was carried out using the seamless mosaic tool in ENVI 5.6 software based on the bilinear interpolation resampling method.

In order to obtain the height data of the objects, the DTM data expressing the earth's surface height was subtracted from the DSM, which shows the height of the objects or terrain surface. DSM was created from the first return LiDAR pulses by producer, which can be reached any objects or directly earth's surface without touching an object. The result of subtraction is called normalised DSM (nDSM) and represents the object's actual height as it refers to the height of objects from the ground surface. In the next step, it was observed that there were values below zero in the nDSM data. Then, these noise cells were removed. These processes were executed using the raster calculator tool in ArcGIS software.

In the next step, the ECW files which each one of them correspond one 2019 vertical aerial photograph were mosaicked. The data were first mosaiced in ENVI 5.6 using a seamless mosaic tool based on nearest neighbour resampling method to create an image of five-by-five km grid tile areas. Afterwards, these six grid tiles images were mosaiced in the same way, and 2019 vertical aerial photography was obtained as a single TIF file.

Subsequently, 2018 nDSM was georeferenced into the British National Grid coordinate system using 2019 vertical aerial photography, and 2014 nDSM was georeferenced using the 2013 CASI multispectral imagery with the define projection tool in ArcGIS Pro software. 2018 nDSM data were resampled to obtain same resolution LiDAR and aerial image data, using the resample tool in ArcGIS software according to the bilinear method. Thus, DEM and aerial imagery with 0.2 m spatial resolution for 2018/2019 and 1 m spatial resolution for 2013/2014 were obtained.

In the final stage of pre-processing, using the extract by mask tool in ArcGIS Pro software, non-overlap areas of 2018 DEM and 2019 vertical aerial photography data were extracted from each other. The same process was applied to the 2014 DEM and 2013 CASI multispectral imagery. Thus, the pre-processing phase was completed, and the datasets were set for segmentation, which is the first stage of OBIA.

3.5. Segmentation

Image segmentation is a technique for dividing an image into objects based on homogeneity (Pal and Pal, 1993) and the essential and critical step of OBIA (Blaschke et al., 2008). The accuracy of object-based classification largely depends on the image object's precision, also called a segment (Mountrakis et al., 2011). There are two main principles of image segmentation, top-down and bottom-up, respectively, depending on whether the recorded object representations are used in segmentation or not (Borenstein and Ullman, 2008). In the eCognition software, four types of top-down segmentation algorithms are offered to the user, namely chessboard, quadtree-based and contrast filter and contrast split segmentation algorithms. While producing rectangular segments with chessboard and quadtree-based algorithm, the contrast filter and the contrast split algorithms are suitable for studies where contrast difference is the determining feature in classification. Therefore, top-down segmentation algorithms were not chosen to segment the data for this study. Multi-threshold, spectral difference and multiresolution segmentation algorithms are presented to the user as bottom-up algorithms (eCognition Developer, 2014).

In this project, the multiresolution segmentation (MRS) method was applied. MRS has been the most common and one of the most successful image segmentation algorithms (Witharana and Civco, 2014). Moreover, MRS performs strongly to segment vegetation bodies (Munyati, 2018).

MRS combines neighbouring pixels with similar colour, shape, and texture properties to create homogeneous image objects (Baatz, 2000). This process occurs through three parameters: shape, compactness, and scale. The shape value expresses the textural homogeneity of the result image objects. It is calculated by the sum of the smoothness and compactness values of the possible image objects to be formed a result of segmentation. According to the shape parameter value determined for segmentation, image objects with optimum smooth border and overall compactness values are created from pixels. Colour and shape values are inversely proportional to complement each other and affect the segmentation process. For example, if the shape value is 0.9, the colour effect on the segmentation, that is, the effect of digital numbers (DN), will be 0.1. If the shape value is selected as 0.5, the pixels will be segmented as image objects with equal weights of colour and shape (Definies, 2007). However, the scale parameter is considered the most crucial parameter in segmentation because it controls the average object size (Lowe and Guo, 2011). Smaller scale parameter value, a higher number of objects (Laliberte and Rango, 2009).

The segmentation processing time of the entire study area takes a long time due to the size of the dataset. To save time and get more effective results, test areas (Figure 3.4 and 3.5) comprised by public and private green spaces and residential zones were selected from both data sets.

Figure 3.4 Test area from 0.2 m spatial resolution image for segmentation process

Figure 3.5 Test area from 1 m spatial resolution image for segmentation process

These test areas were segmented using the "Automated Estimation of Scale Parameter Tool (Automated ESP)" , aka ESP-2 tool developed by Drăguţ et al. (2014) to use in eCognition software. With ESP-2 tool the scale parameter (SP) is determined for multiresolution segmentation of more than one layer.

Each layer, each of the aerial image spectral bands and nDSM data for this study, was iteratively segmented according to multiresolution segmentation. In this iterative process, the SP value increases constantly. The iteration is terminated if the average local variance of the layers in a SP value is lower or equal to the previous scale. This SP is assigned as level one, two or three based on the order. According to this algorithm, three levels of optimal scale are determined for the area to be segmented (Drăguţ et al., 2014).

To choose the optimum SP, parameters were kept as default while using the tool as suggestion of Drăguţ et al. (2014), except shape and compactness. Shape and compactness values range between 0.1 and 0.9 (Definienns, 2007). The tool was performed with shape and compactness values of 0.1, 0.5 and 0.9 of input datasets, firstly, for vertical aerial photography and 2018 nDSM, then for CASI multispectral image and 2014 nDSM as nine different combinations. The SP values and the number of objects resulting from the SP estimation are obtained for three different levels (Table 3.7 and 3.8, Appendix 1 and 2). The results were analysed whether each real object was segmented as a separate object. For example, attention was paid to whether the road, private gardens, buildings, and open green spaces are separate image objects. As a result, it has been observed that the Level-2 results (Figure 3.6 and Table 3.7) for the 0.2 m resolution dataset and Level-3 SP values for the lower spatial resolution dataset consist of a suitable number of image objects for the purpose of the study (Figure 3.7, Table 3.8).

Table 3.7 Estimated scale parameters and number of objects for 0.2 m resolution data (Level 2)

Compactness (0.1 – 0.9)	**Shape (0.1 – 0.9)**	**Scale Parameter**	**Number of Objects**	**Figure**
0.1	0.1	113	55	Figure 3.6 (a)
0.1	0.5	174	22	Figure 3.6 (b)
0.1	0.9	87	18	Figure 3.6 (c)
0.5	0.1	128	52	Figure 3.6 (d)
0.5	0.5	138	37	Figure 3.6 (e)
0.5	0.9	76	39	Figure 3.6 (f)
0.9	0.1	123	56	Figure 3.6 (g)
0.9	0.5	138	39	Figure 3.6 (h)
0.9	0.9	61	73	Figure 3.6 (i)

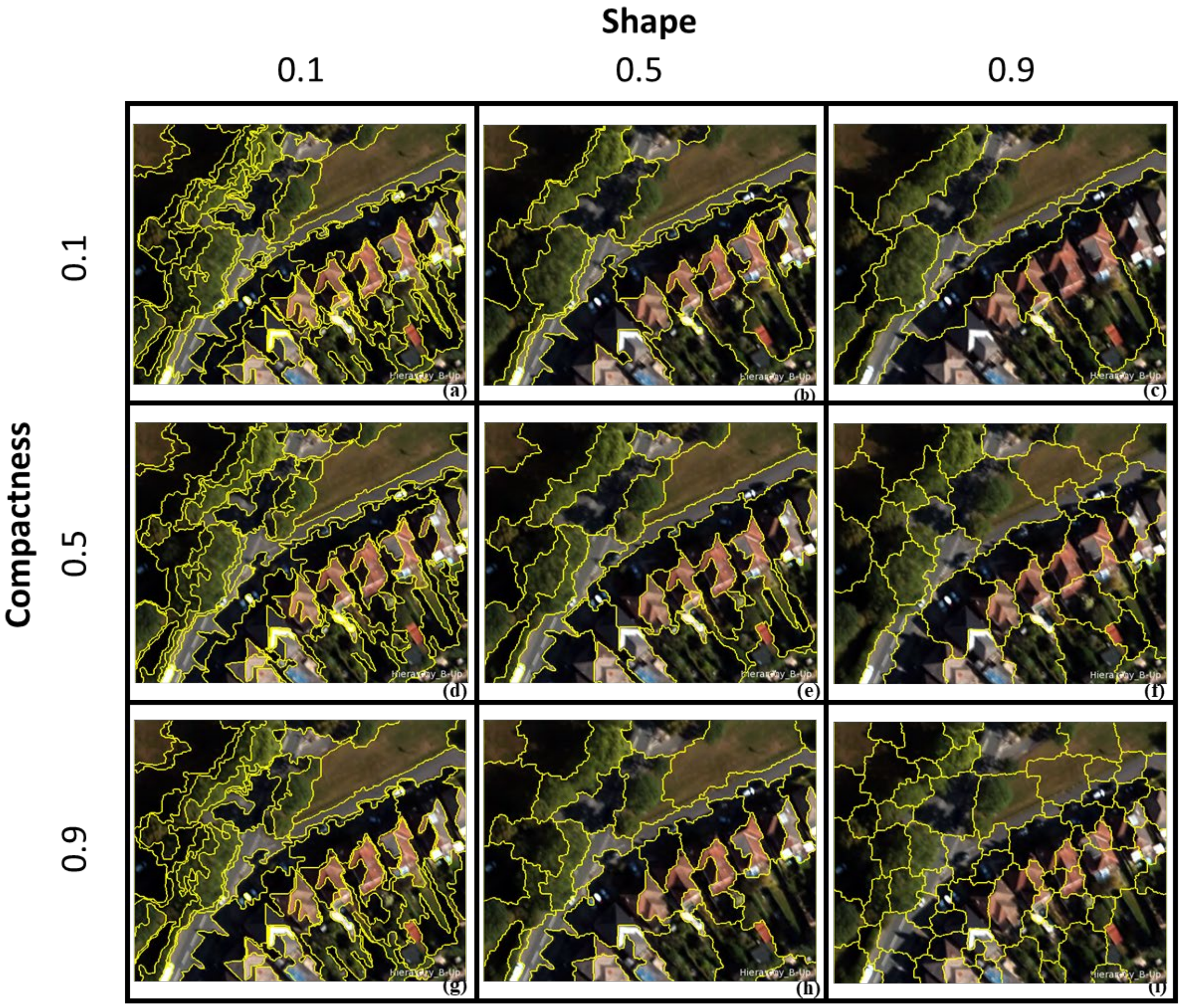

Figure 3.6 Segmentation result of the 0.2 m spatial resolution (Figure 3.4) data

Figure 3.6 (e) shows the most appropriate segments among these nine segmentation combinations and the SP value is 138. While compactness is 0.9 and shape is 0.5, the obtained SP value is also 138, however the number of objects is different (Figure 3.6(h)). Number of objects could be different for the same area with same scale parameter values (Table 3.7). While choosing the SP, shape and compactness values for segmentation, results were evaluated visually. The values at which the most suitable segmented image was obtained were selected for the purpose of the study. For 0.2 m spatial resolution data, scale parameter 138, shape and compactness values selected as 0.5 (Figure 3.6 (e)), because according to aim of the project, each dwelling should be segmented as a different image objects. Also, trees must be segmented different from other vegetation.

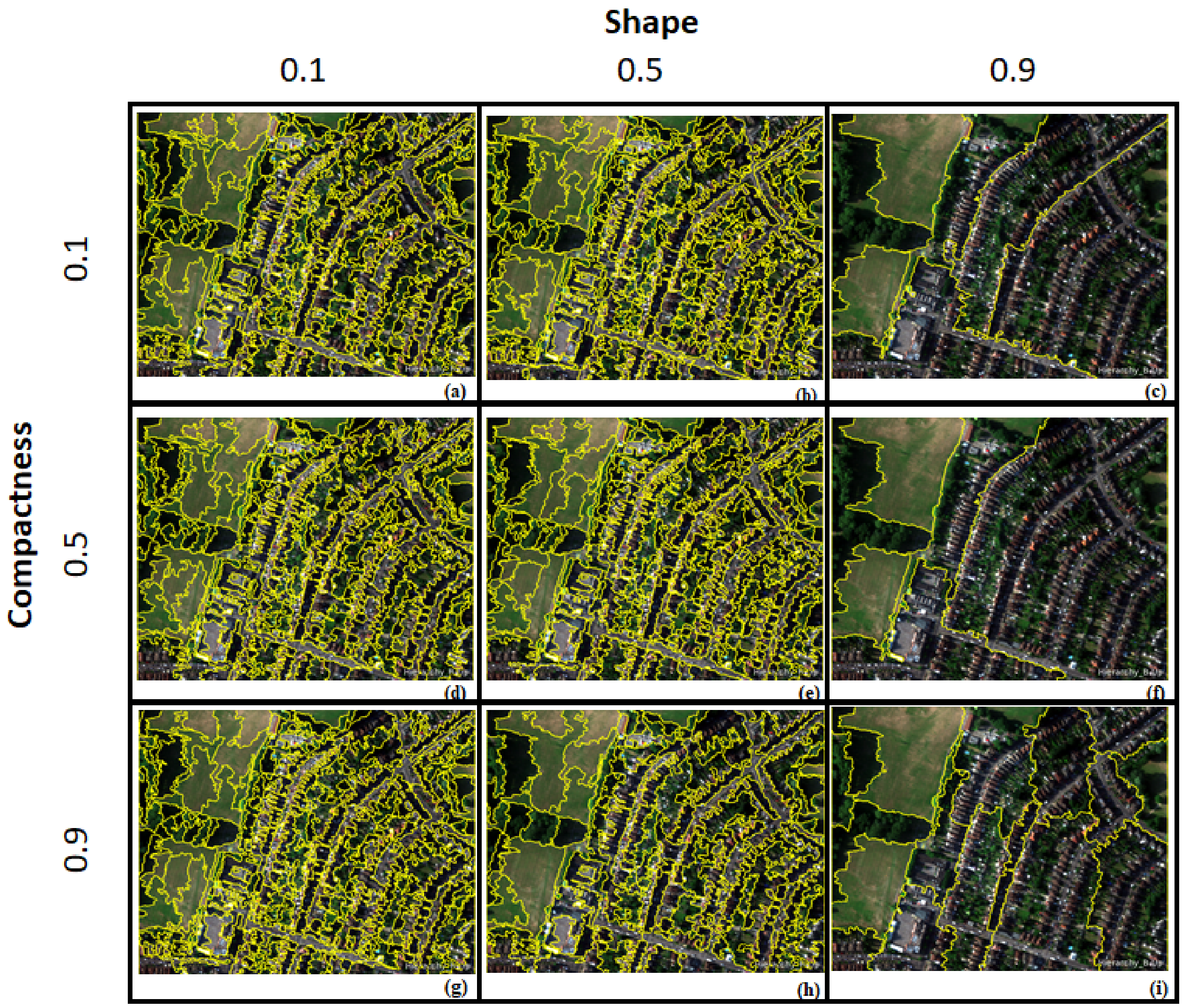

Figure 3.7 Segmentation result of the 1 m spatial resolution (Figure 3.5) data

For the 1 m resolution dataset, compactness 0.9, shape 0.5 scale parameter 324 (Table 3.8), which distinguishes real objects from each other and is a significant number of objects for classification, is selected. As seen in the figure (Figure 3.7), when shape parameter selected 0.9 regardless the value of compactness, the segmented images relatively similar than other shape values' results, and block of dwellings comprised by only one or a few image objects.

Table 3.8 Estimated scale parameters and number of objects for 1 m resolution data (Level3)

Compactness (0.1 – 0.9)	Shape (0.1 – 0.9)	Scale Parameter	Number of Objects	Figure
0.1	0.1	326	142	Figure 3.7 (a)
0.1	0.5	212	214	Figure 3.7 (b)
0.1	0.9	404	7	Figure 3.7 (c)
0.5	0.1	297	179	Figure 3.7 (d)
0.5	0.5	226	177	Figure 3.7 (e)
0.5	0.9	402	6	Figure 3.7 (f)
0.9	0.1	276	209	Figure 3.7 (g)
0.9	0.5	324	85	Figure 3.7 (h)
0.9	0.9	291	18	Figure 3.7 (i)

3.6. Object-based Image Classification

Assigning a class to the image objects can be done with two different approaches: nearest neighbour (NN) and membership function, alias rule-based classification (Myint et al., 2011).

Firstly, supervised NN classifier method tested on the study area using the recent, higher resolution data. While samples were selecting, UK national land use and land cover (LULC) classification report prepared by Harrison (2006) was followed. According to the report, public car parks, roads, railways, airports, and docks are a part of the transport land use class. For this reason, these objects are accepted as belonging to the road class as assets that part of the same LULC class during classification and accuracy assessment.

NN assigns class to segments based on the similarity of selected samples (Hodgson et al., 2003). However, the accuracy of the classification depends on the characteristics of the samples, which are the main disadvantage of this approach. Also, in the segmentation and classification of the study area directly, only the segmentation process took hours. Nevertheless, greenspaces could be classified as private and public directly from supervised classification based on training samples, so that UGSs would be classified as private and public without the need for post-processing. However, the result obtained in this case would not be independent of personal interpretation and subjectivity. Furthermore, the successful implementation of such an approach would be valid in cases where classification was made by someone who has knowledge of the study area and public and private greenspaces could be separated by visual interpretation.

In addition, to develop a standard methodology to be used in the mapping of green areas in the city with the OBIA technique, instead of subjectively selecting and classifying training samples depending on the user, a rule-based classification method was preferred with high applicability for different data sets by creating a ruleset. Rule-based approach enables user to examine the spatial and spectral characteristics of segments when defining the class rule conditions (Xu, 2013). However, which classification results will be used to separate the green areas in the city was decided by comparing the overall accuracy and kappa values of the supervised and rule-based classification results.

Figure 3.8 True colour image of the test area for 0.2 m spatial resolution data

Secondly, the test area has been selected based on consists of similar features as the study area, such as residential and industrial non-residential buildings, river, roads, railway, stadium, public car parks, docks, trees, private grassland (Figure 3.8). Then, ruleset approach was carried out on the test area of finer resolution dataset two times. Two different rule sets and classes (Figure 3.9 and 3.10) were chosen based on trial-and-error base to decide the most appropriate one.

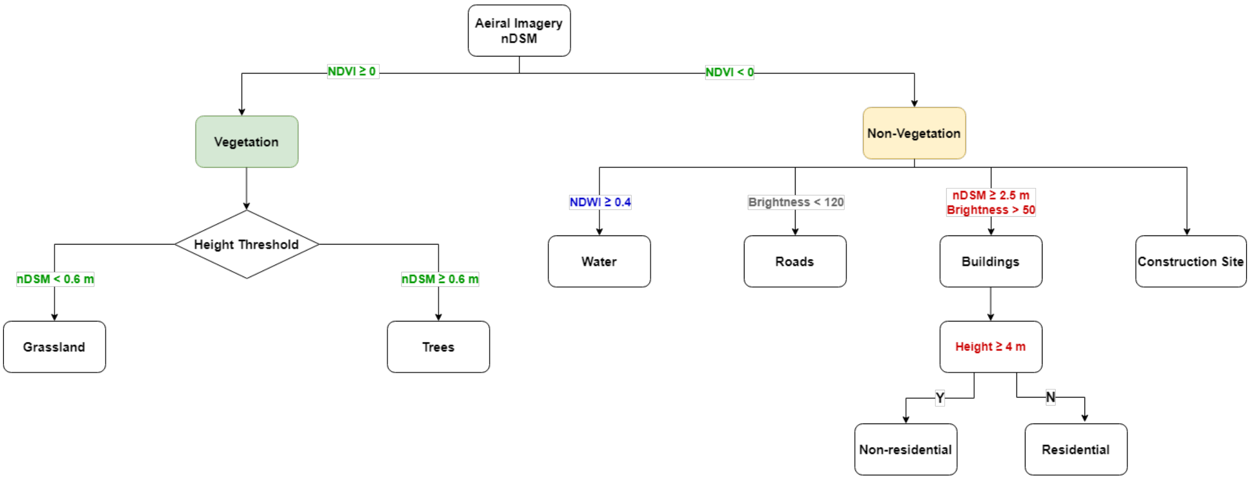

Figure 3.9 First Ruleset of Rule-based Classification

$$\boldsymbol{NDVI} = \frac{\textbf{NIR}-\textbf{RED}}{\textbf{NIR}+\textbf{RED}} \qquad \textbf{(Equation 1)}$$

$$\boldsymbol{NDWI} = \frac{\textbf{GREEN}-\textbf{NIR}}{\textbf{GREEN}+\textbf{NIR}} \qquad \textbf{(Equation 2)}$$

While determining the rulesets, it is planned to separate vegetation from non-vegetation areas in the first stage. For this purpose, the Normalized difference vegetation index (Equation 1), proposed by Rouse et al. (1974), was used. NDVI ranges between -1 and 1. Positive values represent vegetation, and increasing positive values indicate an increase in the amount of green (Chuai, 2013).

Afterwards, image objects that were not classified as vegetation were divided into water and both water and others according to the NDWI formula (Equation 2) proposed by Gao (1996). Although positive NDWI values indicate whether a place has water features, NDWI values of image objects in the test area were examined before set the threshold NDWI value. It was observed that NDWI values of some non-water features between 0 and 0.4. Then, NDWI threshold selected 0.4 to detect water features.

While the vegetation class is divided into grassland and tree, when the nDSM values of vegetation objects that do not include trees are considered, the height threshold value was decided 0.6 m.

In unclassified objects remaining after classification of water and vegetation, it has been observed that places with relatively lower brightness values are commonly roads since the roads are in shadow in the test area. Objects with a brightness value below 120 were classified as roads. The brightness value is calculated as the average of the digital number (DN) values of the spectral bands (eCognition Developer, 2014). In this case, red, green, blue and NIR bands of the 0.2 m spatial resolution data.

In the next step, the buildings were classified into two different classes, residential and non-residential, according to their height and spectral information using the brightness and the nDSM values. It has been observed from the image that the remaining unclassified objects are part of mainly in construction sites. Then, these objects were classified as a construction sites.

Since residential areas occupy much less space than the real situation and are represented by only two reference points out of 100, and only one of them has been correctly classified (Appendix 4), a new ruleset has been determined (Figure 3.10). It is necessary for the aim of the study because the residential area class will be the most decisive parameter in separating the public and private areas.

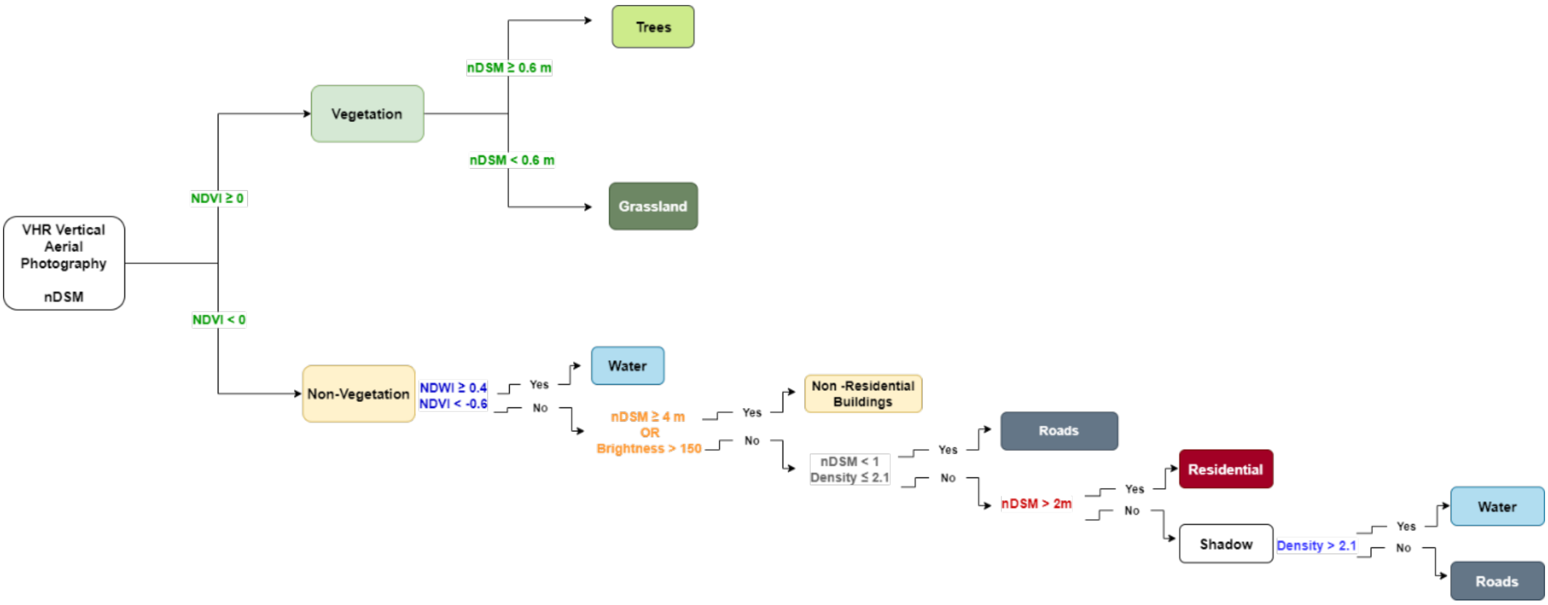

Figure 3.10 Second Ruleset of Rule-based Classification

To set different ruleset for OBIA, vegetation and non-vegetation areas differentiate each other with same rule with NDVI because these areas were classified relatively higher accurate than others, especially grassland (Appendix 4). However, to assign water class NDVI and NDWI values were used together, particularly to classify wetland area more accurate. Later, unclassified image objects classified as non-residential areas initially with using height (nDSM) and brightness values because non-residential areas can be differentiated other unclassified parts particularly based on the object heights and brightness values. Then, roads class was assigned based on nDSM and density values. Density shows the spatial distribution of pixels in segments, it is calculated by dividing the image object`s area by average of the axes of ellipse fitted to the segment (eCognition Developer, 2014). The reason of density value used for assigning the road class is the horizontal shape of the roads, some image objects which depicts roads have less density value than other segments. Once roads classified, unclassified segments mainly show residential areas and height information was used to classify residential areas. Lastly, rest of the image objects evaluated as shadow. As a last step, density threshold, which has already used for assign roads class, was used to separate shadow regions water and roads. Decided thresholds values shown in Table 3.9.

Table 3.9 Threshold values for Ruleset Classification

Class	**Threshold Value (Mean Layer Value of Image Objects)**
Grassland	NDVI $\geq$ 0 & nDSM < 0.6 m
Trees	NDVI $\geq$ 0 & nDSM $\geq$ 0.6 m
Water	NDVI < 0.6 & NDWI $\geq$ 0.4 Density > 2.1 of Shadow Class
Non-residential	nDSM $\geq$ 4 m & Brightness > 150 (8-bit data) Brightness > 1200 (16-bit data)
Roads	nDSM < 1 m & Density $\leq$ 2.1 Density $\leq$ 2.1 of Shadow Class
Residential	nDSM > 2 m
Unclassified = Shadow	Classified Water and Roads based on Density Value

Classification results of the test area are shown in Figure 4.1. Visually, second ruleset shows better performance particularly for residential areas. However, accuracy assessments were carried out to compare accomplishment of rulesets quantitively.

To make accuracy assessment ArcGIS Pro software was used, classified image objects export from eCognition to ArcGIS Pro. Then, 100 random points, which are at least 0.2 m apart from each other to create at most one point for one pixel, created in the test area separately and classified image converted vector to raster format. Then, closest to the date the data was obtained from Google Earth image used as a reference data to make accuracy assessment. The results are shown as error matrices (Appendix 3,4,5,6 and 7).

Lastly, same threshold values, except brightness value, were used for classification of coarser resolution dataset on test area (Figure 3.11). While selecting the test area for the classification of the 1 m resolution data set, attention was paid to ensure that it was an area with similar features as the area in the other data set.

Because of the bit size difference of the datasets, brightness threshold selected higher which was selected as 1200, except that the same threshold values (Table 3.9) were applied. The result of the classification and the accuracy analysis are shown in (Figure 4.2, Appendix 5). For accuracy assessment same number of points created but the minimum distance between two points were set as 1 m instead of 0.2. Then, the match of these points in the most recent Google Earth image to the CASI multispectral image were used as reference data.

Finally, classified data of the study area is needed to map distribution of the green space in the study area. Therefore, same methodology was followed to classify the study area with using finer spatial resolution dataset.

Figure 3.11 True colour image of the test area for 1 m spatial resolution data

3.7. Separating Public and Private Urban Green Spaces

The classification results used in the green space analyses were produced as a result of rule-based classification according to the ruleset which named in this study as ruleset-2 by using 0.2 m spatial resolution data. Firstly, the grassland and trees classes in this result are combined as a single class as vegetation to validate green space classification before the step of separating public and private green spaces in ArcGIS Pro.

For the accuracy assessment of residential areas, the reference data, the current OpenStreetMap building location data (Table 3.6) was downloaded from bbbike.org and the residential areas field in this data was used in the validation calculation. For green spaces, OS Master Map Green space - Layer data downloaded from digimap.com is used as reference data.

In separating green spaces as public and private, it is decided according to the location of green spaces relative to residential areas. Therefore, firstly, calculation of the classifications of vegetation and residential areas are assessed.

To define the green spaces in the study area before the analysis of the separation of public and private green spaces, areas not defined as green space both in OS Master Map Green space – Layer ve OS Open Green spaces reference data, where also nor publicly accessible neither private green space status. These regions were manually eliminated if classified as trees or grassland. Besides, OS Master Map Green space data includes “Beach and Foreshore” data as well as green areas. These, the primary function of which is expressed as “Beach and Foreshore” in the data, were extracted from the OS Master Map Green space – Layer data.

Although it is an accuracy assessment method to select random points and perform the accuracy test of all LULC classes by taking only these points as reference data, there are also area-based accuracy assessment approaches in OBIA (Khatriker and Kumar, 2018; Silver et al., 2019). Accuracies of buildings and green spaces classified in this study were also calculated according to how much area was classified correctly or incorrectly compared to the OpenStreetMap and OS Master Map Green space Layer reference data for the study area.

Areas in which the feature is common in classified and reference data are called true positive (TP), and in classified and reference data, the common areas of the area outside the feature are called true negative (TN). Areas where the non-feature in the reference data is classified as feature are called false positive (FP), and areas classified as non-feature from feature areas are called false negative (FN) (Rutzinger et al., 2009). These values were calculated for residential and vegetation areas by using intersect tool in ArcGIS Pro software.

Assessment was carried by calculating true positive rate (TPR), false positive rate (FPR), and overall accuracies using TP, TN, FP and FN values (Equation 3 and 4). In this study, the TPR value is an indicator of how likely the objects classified as vegetation or building are vegetation or building on an area basis. FPR is the rate of misclassification by area of objects classified as vegetation or building.

Table 3.10 Confusion matrix of the study area rule-based classification

		Reference Data	
		Positive	**Negative**
Classified	**Positive**	**True Positive**	**False Positive**
	Negative	**False Negative**	**True Negative**

$$\textbf{True Positive Rate (TPR)} = \frac{\textbf{TP}}{\textbf{TP+FN}} \quad \textbf{False Positive Rate (FPR)} = \frac{\textbf{FP}}{\textbf{FP+TN}} \qquad \textbf{(Equation 3)}$$

$$\boldsymbol{Accuracy} = \frac{\textbf{TP+TN}}{\textbf{(TP+FP+TN+FN)}} \qquad \textbf{(Equation 4)}$$

Then, it was decided whether the green spaces should be public or private areas according to the spatial proximity relationship between the residential and the vegetation areas. Therefore, it is calculated whether the green areas closest to the residential buildings are concentrated in a certain direction according to the dwellings, with the Euclidean direction tool in ArcGIS software. As a result, it has been calculated that the green areas closest to the residential buildings in the study area are not concentrated in a certain direction facing the dwellings (Figure 4.10).

After it was determined that the green areas were not concentrated in a specific direction according to the buildings, it was decided to calculate whether a green area be private or public according to proximity to residential areas. By choosing the sequential threshold values of 10, 15, 20,25,30, 35 and 40 m, it is considered to classify the green areas as private and public. If the green spaces are no further than the threshold distance from the buildings, they were classified as private green space. Rest of UGS was classified as public green space.

To evaluate the accuracy of the calculated public and private fields, the extent to which the calculated fields intersect with the reference fields was calculated by using the OS Open Green space map as public green space reference data and private garden field of the OS Master Map Green space Layer with using intersect tool in ArcGIS Pro.

The accuracy of the threshold values for public and private green spaces was calculated as the ratio of the overlap area of calculated UGS areas and reference data to the calculated UGS areas. (Figure 4.11).

Consequently, the value that leads to the conclusion that the accuracy rate calculated using the reference data for private and public green spaces is the closest to each other has been accepted as the threshold value for separation public and private green spaces.

Afterwards, for the analysis of the distribution of public and private UGS in the study area, same size the 25 km^2 SU31SE and SU41SW grid tiles, which constitute 95.32% of the study area in total (Table 3.1), were compared to private and public green space presence calculated using the threshold distances.

Finally, maps of distribution of public and private green space were produced for threshold values and reference data (Figure 4.15 and 4.16). Trees in the study area was mapped in the ArcGIS environment by using the point of gravity centres of image objects classified as trees achieved from eCognition software (Figure 4.17).

4. RESULTS

This chapter aims to present the results of the methodology followed with maps, charts, tables, and numerical expressions.

In Section 4.1, the results of object-based image classifications performed with the methodology followed in this study will be presented and the accuracy of these results will be compared. The results of the calculated public and private green spaces and the distribution of tree density will be evaluated quantitively and visualised in Section 4.2.

4.1. Object-based Classifications and their Accuracy Assessments

The overall accuracy and kappa coefficient values of the object-based classification of the test areas and the study area performed in this project are shown in Table 4.1.

Overall accuracy is an indicator of how accurately the data is classified. Kappa coefficient shows the agreement between the classification and the reference value and takes values between 0 and 1. It is a numerical comparison of overall accuracy and random chance of classification. The closer the Kappa value is to 1, the higher the agreement (Landis and Koch, 1977). There is no classification with a kappa value higher than 0.8, that is, with very good accuracy.

When the same classification criteria (ruleset 2) applied, the overall accuracy of the test area is 10% higher than the study area for same resolution (0.2 m) image. Besides, the kappa coefficients of the classifications are 0.78 for the test area while it is 0.66 for the study area. On the other hand, the overall accuracy and kappa values are much lower in lower resolution data (1 m spatial resolution) when classified with the same ruleset, 40% and 0.29 respectively.

Table 4.1 Overall accuracy and Kappa coefficient values of OBIA classifications in this study

Area	Supervised Classification	Rule-based Classification	
		Ruleset 1	Ruleset 2
Test Area of 0.2 m resolution data		Overall Accuracy: 75% Kappa: 0.69	Overall Accuracy: 82 % Kappa: 0.78
Test Area of 1 m resolution data			Overall Accuracy: 40 % Kappa: 0.29
The Study Area 0.2 m resolution data	Overall Accuracy: 67% Kappa: 0.61		Overall Accuracy: 72% Kappa: 0.66

With the rule-based approach, when the same area (Figure 3.8) was classified using different numbers of classes and, more importantly, different ruleset, the second ruleset performs better. For the test area of finer resolution data, the overall accuracy and kappa coefficient for ruleset 2 are 82% and 0.78, respectively, while these values are 75% and 0.69 when ruleset1 is applied (Figure 4.1).

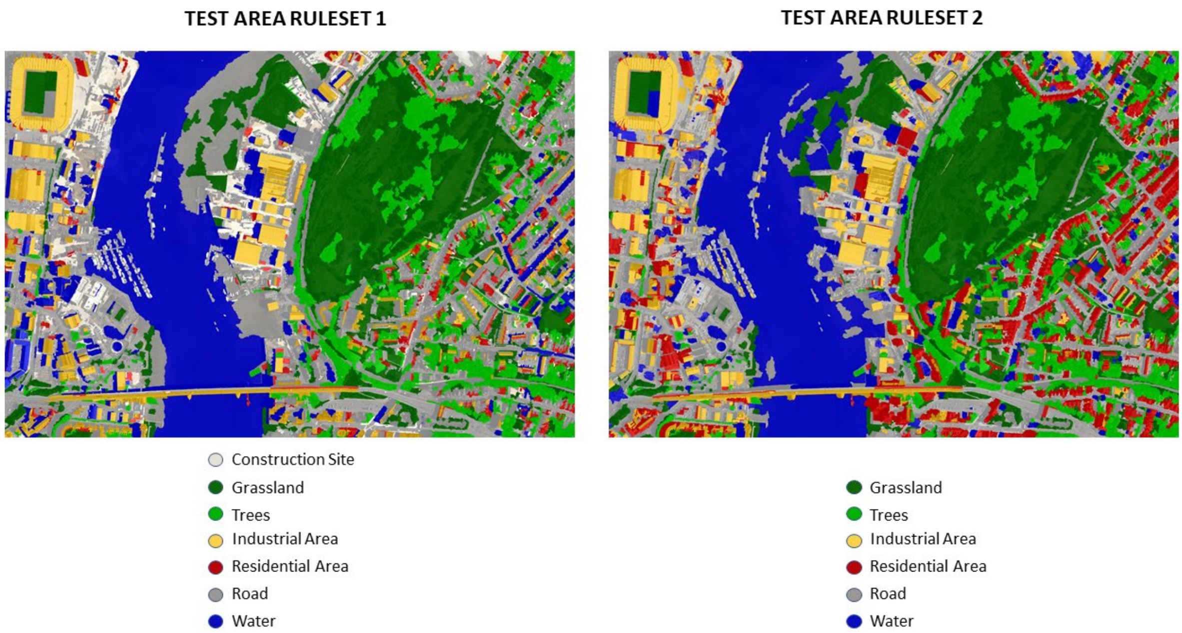

Figure 4.1 LULC maps of the test area of 0.2 m spatial resolution data

The lowest and highest accuracy among the classifications was obtained by using the "ruleset-2" threshold values. The overall accuracy of test area of 1 m resolution data is 40% and the kappa coefficient is 0.29. In addition, all residential area points in the reference data were misclassified as trees. On the other hand, overall accuracy of the test area of 0.2 m resolution data with applying the same ruleset is 82% and the kappa value is 0.78 (Table 4.1).

TEST AREA RULESET 2 (1m resolution)

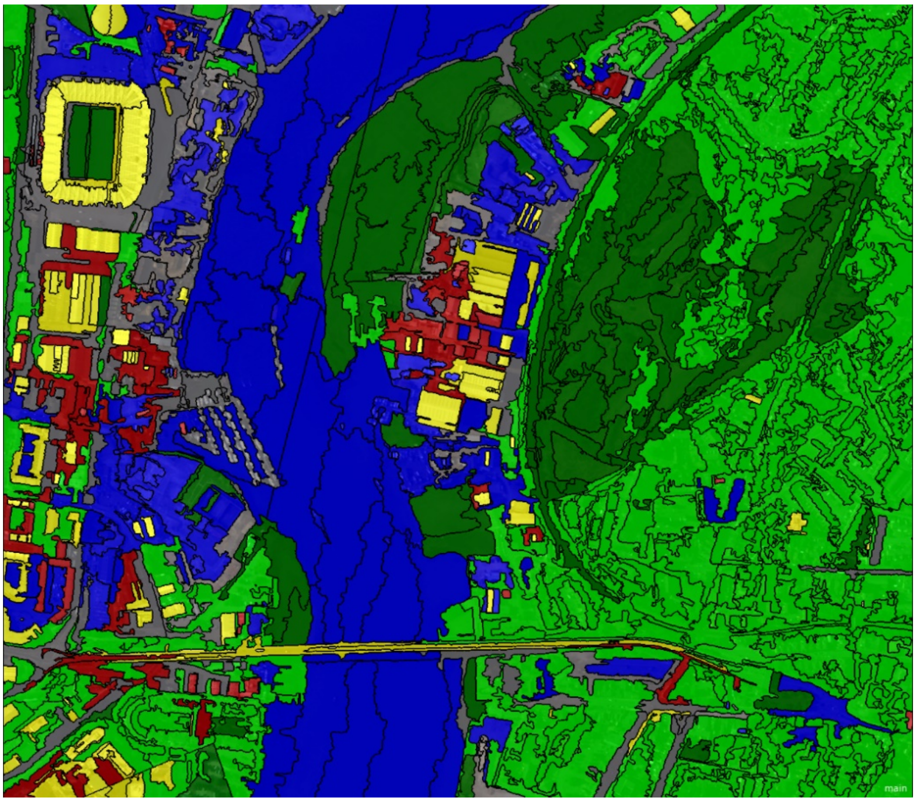

Figure 4.2 LULC map of the test area of 1 m spatial resolution data

In this project, the study area's LULC map was produced with both supervised and rule-based object-based classification, and the overall accuracy of the classification was 72% when the rule-based approach was applied, and 67% in supervised classification (Figure 4.3).

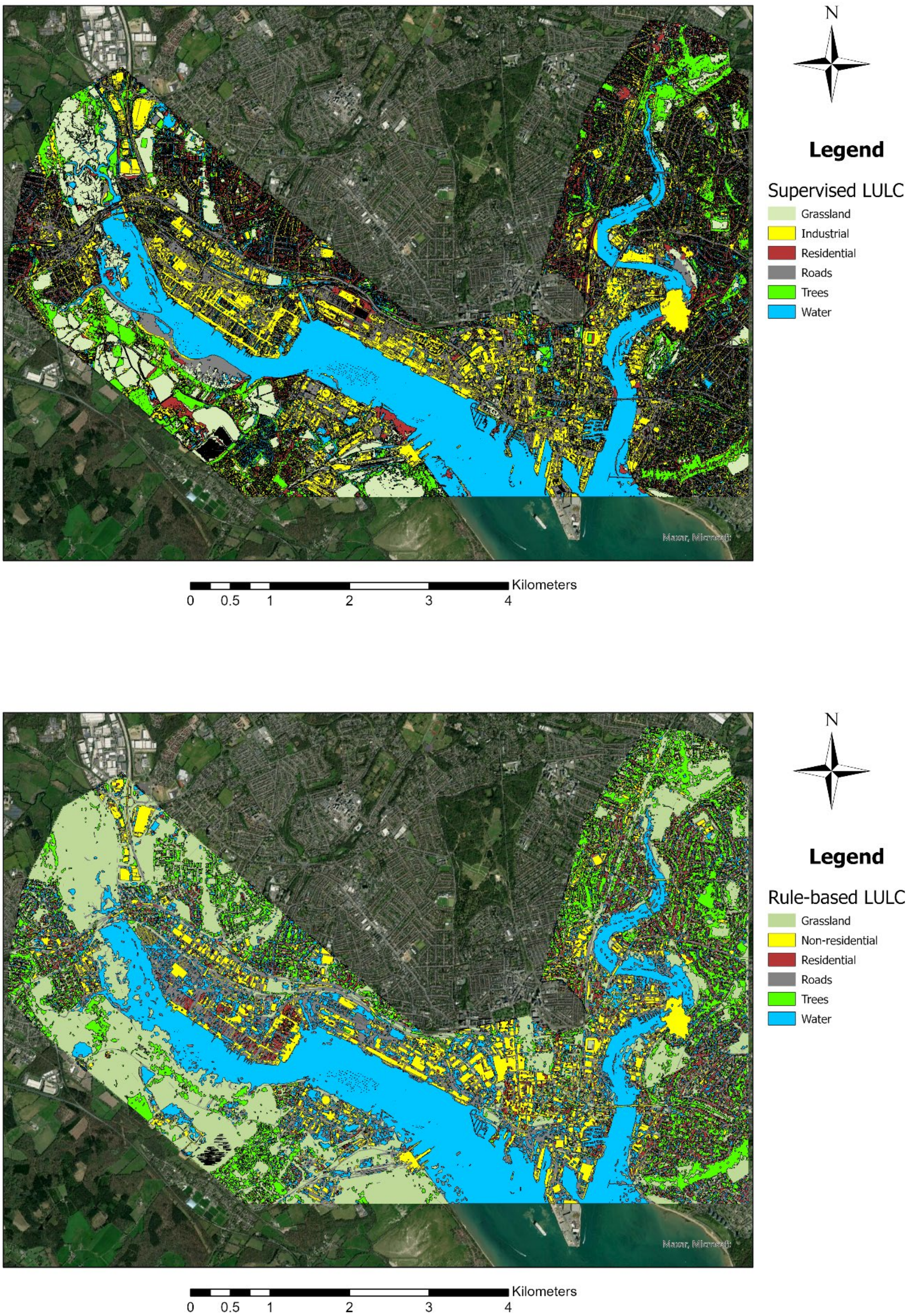

Figure 4.3 LULC maps of Supervised Classification (up), Rule-based (Ruleset2) Classification (down)

There are several reasons of misclassification. Atmospheric distortion is one of them. The images show the true colour composite of finer resolution image and some of misclassified part caused by distortions (Figure 4.4 and 4.5).

Figure 4.4 Atmospheric distortion example

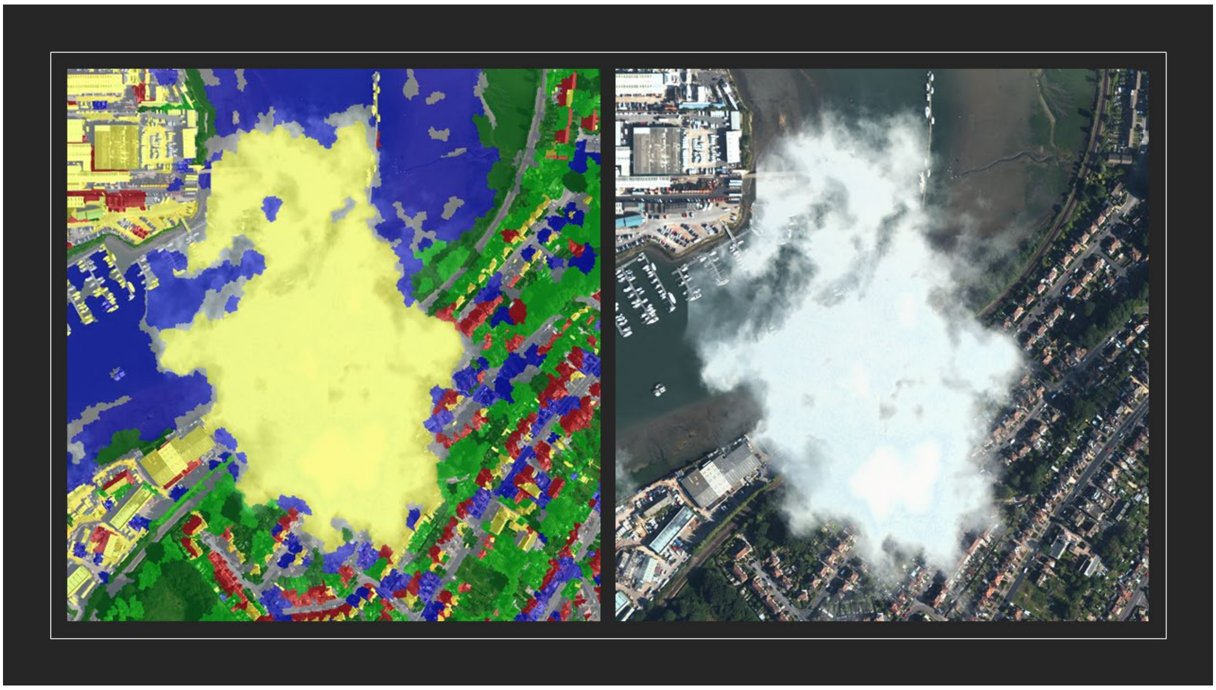

Figure 4.5 Atmospheric distortion example caused by the cloud

Shadows due to height differences caused different objects to be segmented as the same image object, therefore these were classified as same class although they are different features (Figure 4.6).

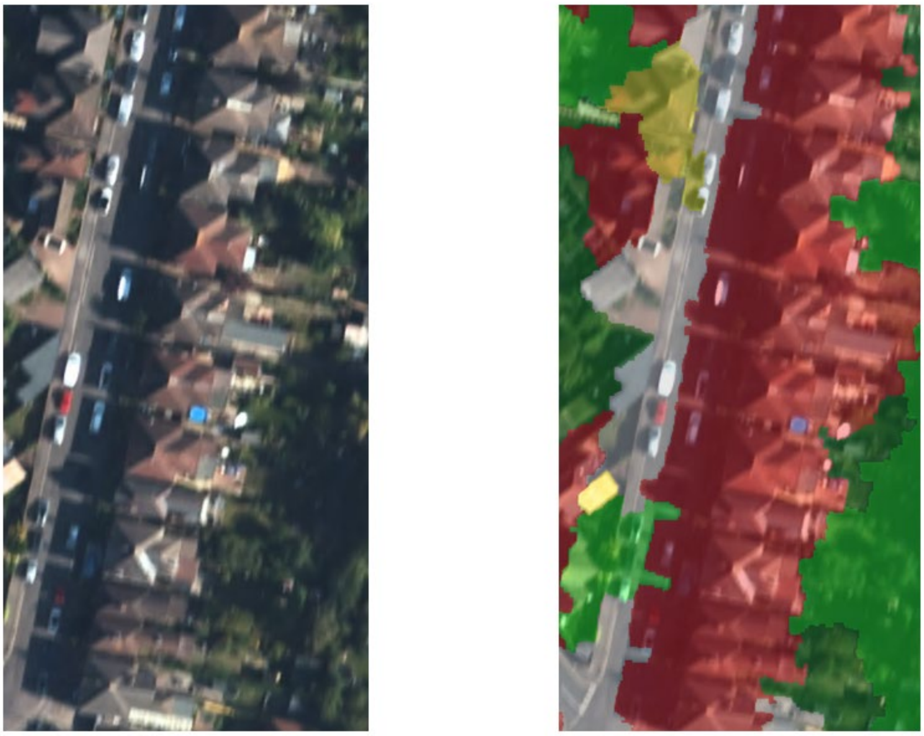

Figure 4.6 Misclassification caused by shadow effect

Port of Southampton covers a remarkable part of the study area. Some containers in this complex structure with many different objects were classified as residential area due to their spatial and especially spectral characteristics (Figure 4.7).

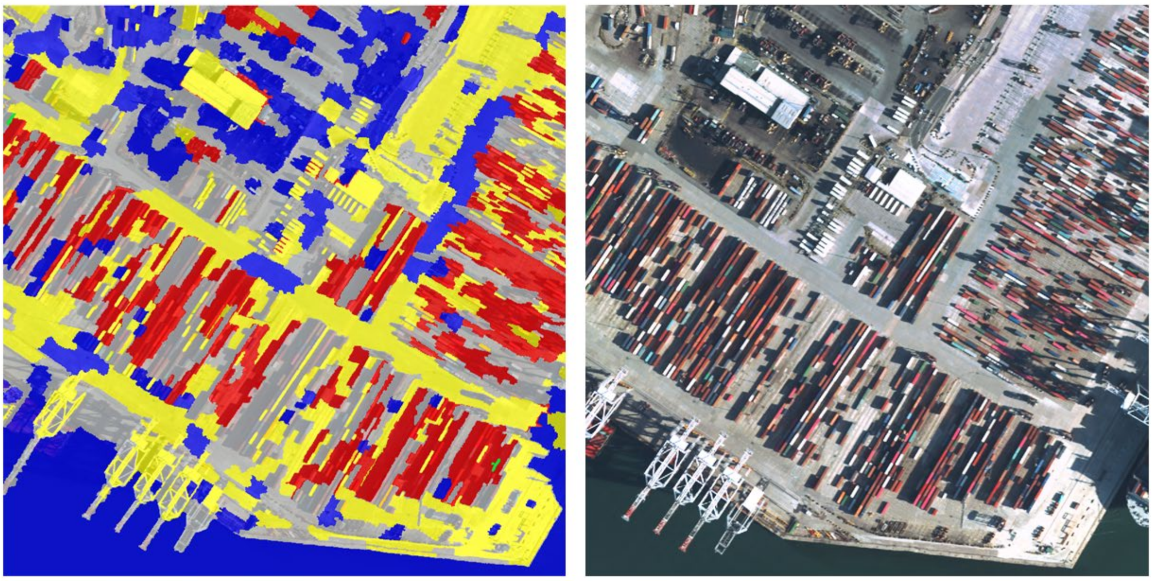

Figure 4.7 Port of Southampton

There are many movable objects in the study area because of nature of cities. These objects, which do not represent any LULC class, caused incorrect classification while generating the LULC map (Figure 4.8).

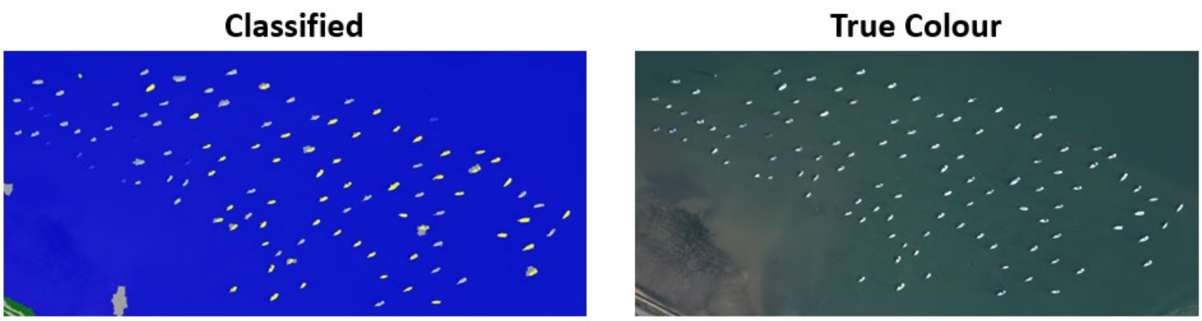

Figure 4.8 Movable features in the study area

According to the result of rule-based classification applied with ruleset 2 on the study area, 1.61 km^2 is classified as residential area although in reference data these are not part of residential area. Nevertheless, the areas not part of the building are classified much more accurately than buildings. While area of 1.05 km^2 classified as another class than the residential area, area of.30.85 km^2 is not a residential area as it is classified (Table 4.2).

Table 4.2 Confusion matrix of building features

		Reference Data	
		Residential Area	**Others**
Classified	**Residential Area**	**True Positive (TP)** 0.56 km^2	**False Positive (FP)** 1.61 km^2
	Others	**False Negative (FN)** 1.05 km^2	**True Negative (TN)** 30.85 km^2

On the other hand, accuracy of green space extraction is higher than residential area. Area of 6.92 km^2 classified as green space, where is green space in the reference data as well. However, 1.59 km^2 green space is misclassified (Table 4.3).

Table 4.3 Confusion matrix of green space (trees + grassland) features

		Reference Data	
		Green space	**Others**
Classified	**Green space**	**True Positive (TP)** 6.92 km^2	**False Positive (FP)** 2.24 km^2
	Others	**False Negative (FN)** 1.59 km^2	**True Negative (TN)** 18.71 km^2

FPR values are relatively lower, which means although they are not dwellings zone nor green space, however not many objects misclassified as residential area or green space. Despite this, TPR value of residential area is lower because of many objects classified as different classes than residential area although these are part of dwellings zone. However, most green space correctly classified therefore the TPR of vegetation is high (Table 4.4).

Table 4.4 True Positive, False Positive and Accuracy rates of residential area and vegetation features

Feature / Accuracy	Residential Area	Vegetation
True Positive Rate	0.35	0.81
False Positive Rate	0.03	0.11
Accuracy	0.92	0.87

4.2. Private and Public Green Spaces and Tree Density

Green space in the study area consists of two type of properties which are grassland and trees (Figure 4.9).

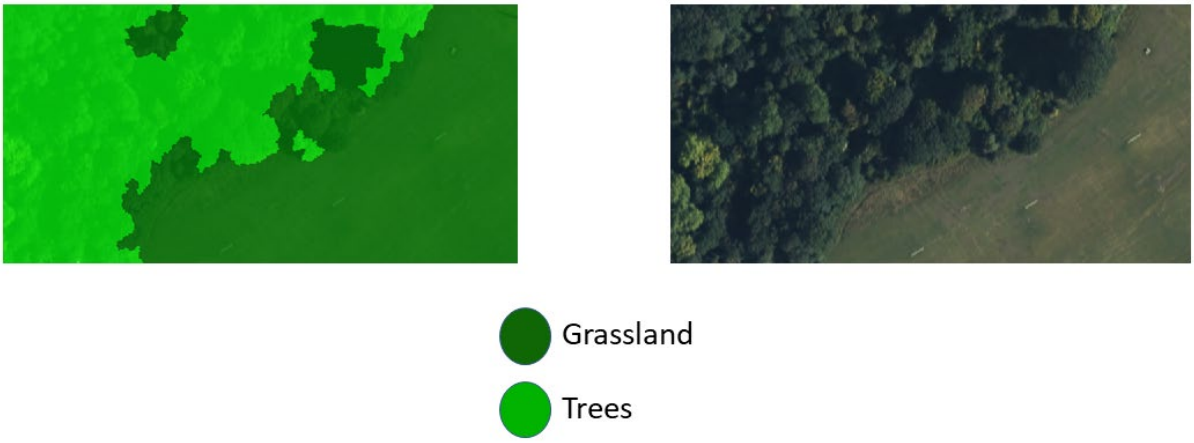

Figure 4.9 Grassland and tree separation

As a result of the Euclidean direction analysis carried out to distribute the green areas as private and public UGS, it was found that the green area closest to the residences can be distributed approximately equally to any aspect of the residence (Figure 4.10).

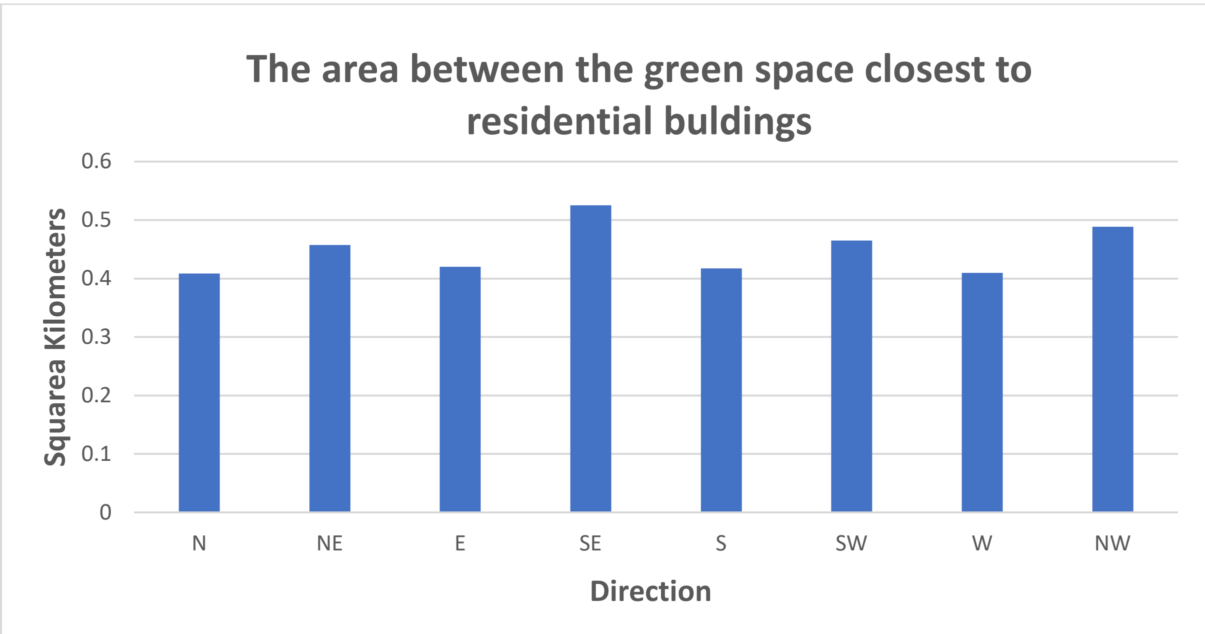

Figure 4.10 Distribution of the green space closest to the dwellings according to the directions in which direction it is

The calculated public and private green spaces cover 3,859,157 m^2 (approximately 3.86 km^2) in the SU31SE, while in the SU41SW they cover 5,306,240 m^2 (approximately 5.31 km^2). These values correspond to 16.4% of the SU31SE and 21.2% of the SU41SW, 25 km^2 grid tiles.

As a result of separating these areas as public and private green spaces according to the determined threshold values, it has been found that the private green space area for the SU31SE grid can vary between 1.69 km^2 and 2.85 km^2, and the public green space can vary between 2.17 and 1 km^2. For the SU41SW grid, private and public green spaces take values between 2.65 and 3.96 km^2 and 2.66 and 1.35 km^2, respectively (Table 4.5).

Table 4.5 Distribution of public and private green spaces in SU31SE and SU41SW grid tiles for each threshold in square meter unit.

Threshold Value	SU31SE Grid Tile		SU41SW Grid Tile	
	Private Green space (m^2)	Public Green space (m^2)	Private Green space (m^2)	Public Green space (m^2)
10 m	1 690 422	2 168 735	2 651 607	2 654 634
15 m	1 971 798	1 887 359	2 980 878	2 325 361
20 m	2 226 149	1 633 009	3 242 103	2 064 138
25 m	2 418 642	1 440 515	3 474 641	1 831 599
30 m	2 579 295	1 279 862	3 656 781	1 649 460
35 m	2 726 618	1 132 539	3 818 265	1 487 975
40 m	2 851 418	1 007 740	3 955 037	1 351 204

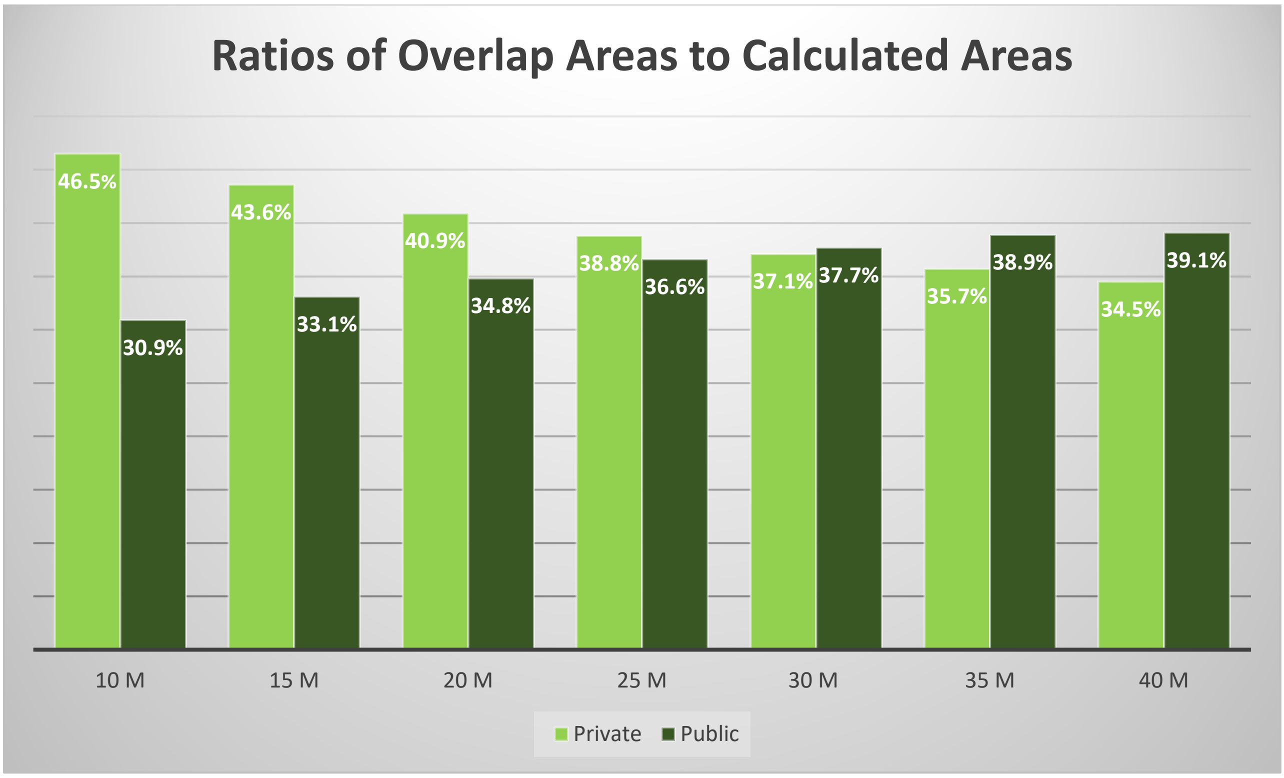

Figure 4.11 The percentages of overlap of public and private green spaces to calculated areas using threshold values

As the selected threshold value increases, the ratio of the intersection of the calculated private green spaces and the reference data to the calculated area decreases, nonetheless it is the opposite for public green spaces**.** In addition, the difference in accuracy values between consecutive threshold values decreased when the threshold value increased until 35 m (Figure 4.11).

Accuracy is the highest when public UGS are defined as green areas at least 40 m from residential areas, highest accuracy for private areas is in the first 10 m from residential areas (Figure 4.11). As a result, a green space is more likely to be private if it is 10 m far or less from a residential building, and public if it is 40 m or more away.

At a threshold value of 30 m, the accuracy rates of public and private green spaces are closest to each other (Figure 4.11). Therefore, the value of 30 m has been accepted as the threshold value for public and private UGS estimation.

Private and Public Green space Distribution in SU31SE grid tile

Figure 4.12 Private and public UGS percentages based on the different threshold values for SU31SE

In Figure 4.12, the percentages of distributions of public and private green spaces according to different threshold values in the SU31SE tile are shown. Only at the 10 m threshold, public UGS are more than private UGS. Private UGS are at the highest rate with 73.9% at 40 m. At the determined threshold value (30 m), private UGS is approximately twice the public UGS.

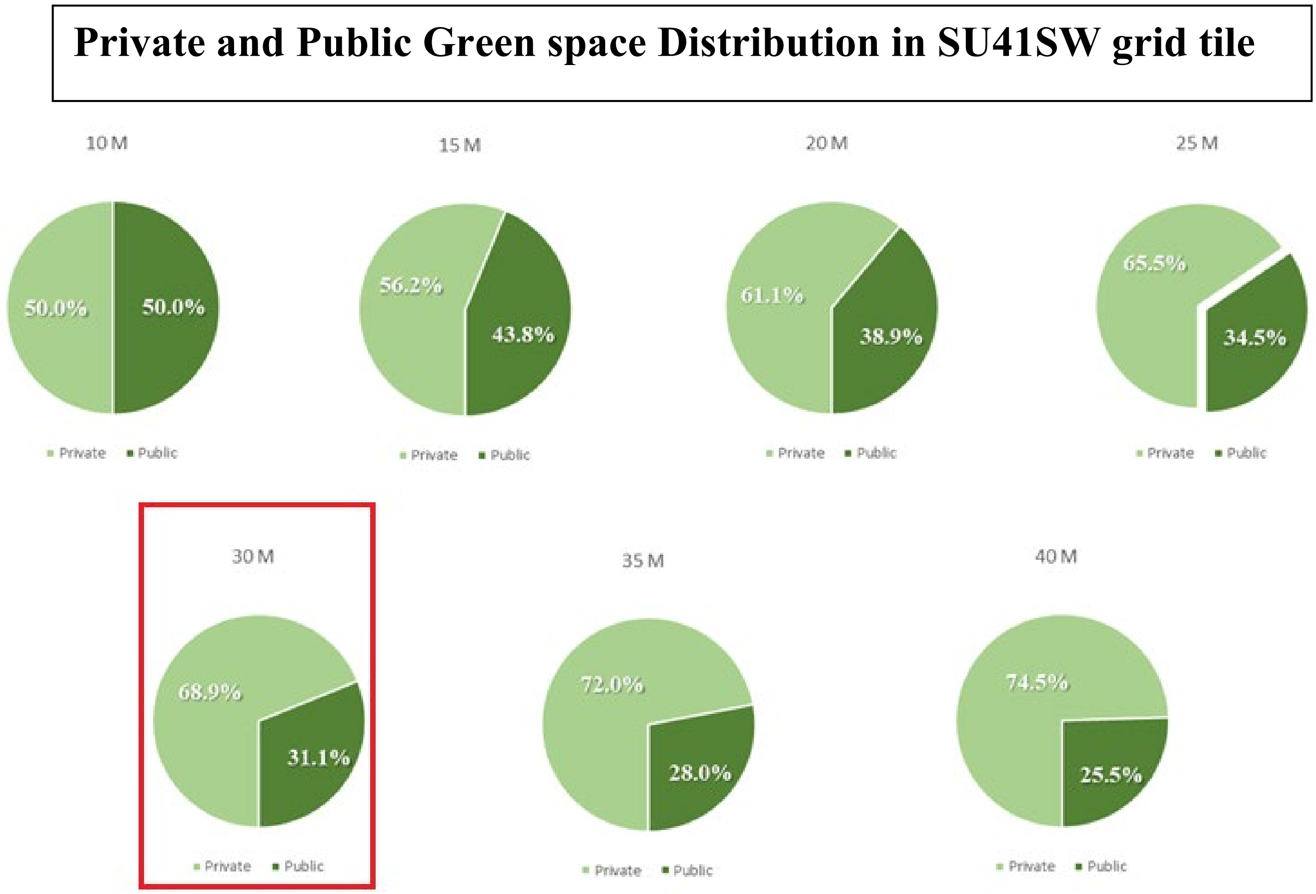

Figure 4.13 Public and private green spaces` percentages based on the different threshold values for SU41SW

The percentages of distributions of public and private green spaces according to different threshold values in the SU31SE tile are shown in Figure 4.13. While the rates of private and public green spaces are equal at the 10 m threshold, the private green spaces are approximately 3 times the size of the public green spaces when threshold estimated as 40 m. At the determined threshold, which is 30 m, the private UGS is more than twice the public UGS.

Table 4.6 Private and public green spaces for the reference data and determined threshold

	SU31SE Grid Tile		SU41SW Grid Tile	
	Private Green space (m^2)	**Public Green space (m^2)**	**Private Green space (m^2)**	**Public Green space (m^2)**
	2 943 197	716 434	5 390 908	1 106 683
In the Study Area	1 199 359	716 434	3 006 159	1 106 683
30 m Threshold	2 579 295	1 279 862	3 656 781	1 649 460

In Table 4.6, how much area the public and private green spaces in the reference data cover in the grids are stated in square meter unit. While there are no public UGS in the area outside the study area within the grid tiles, the private UGS outside the study area is approximately 1.75 km^2 in SU31SE and approximately 2.4 km^2 in SU41SW. According to the reference data, private UGS in SU31SE is more than 4 times of public UGS. In the SU41SW, the private green space is approximately 5 times the public green space (Figure 4.14). According to the reference data, the distribution of private and public green areas in the study area is shown in Figure 4.15.

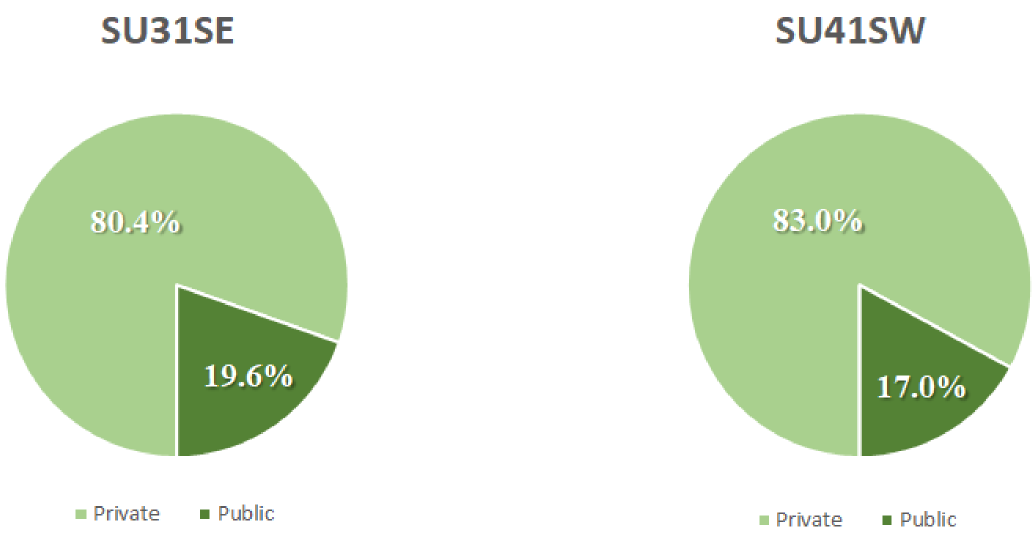

Figure 4.14 Private and public UGS proportions in SU31SE and SU41SW grid tiles.

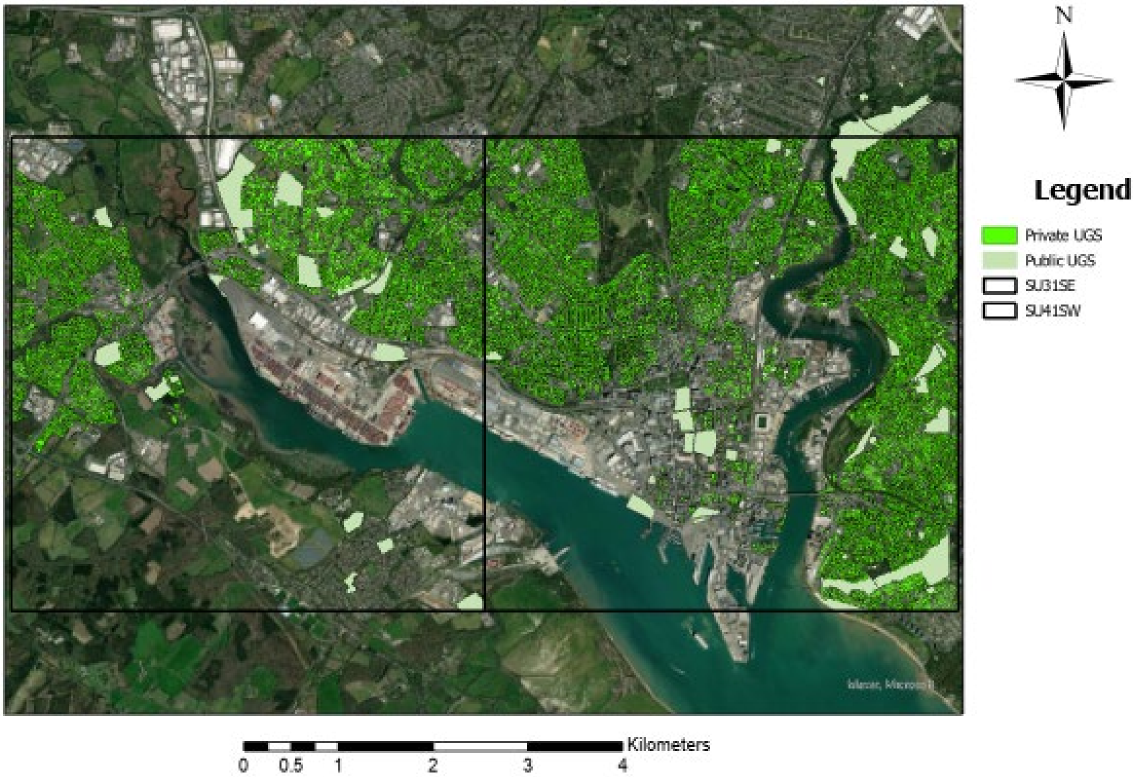

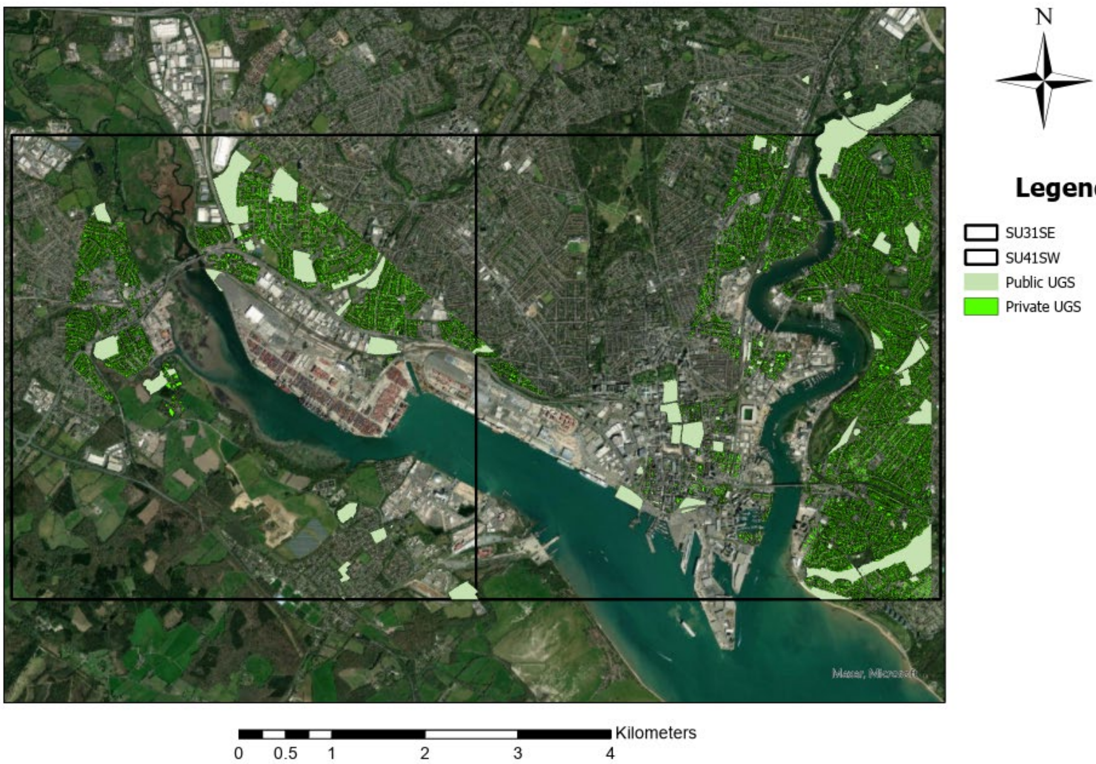

Figure 4.15 Total private and public UGS in the tiles (up), private and public UGS in the study area (down)

The distribution of private and public UGS according to the determined threshold value (30m) and the threshold values of 10m and 40m, where the highest accuracy is calculated for private and public UGS, is shown in Figure 4.16.

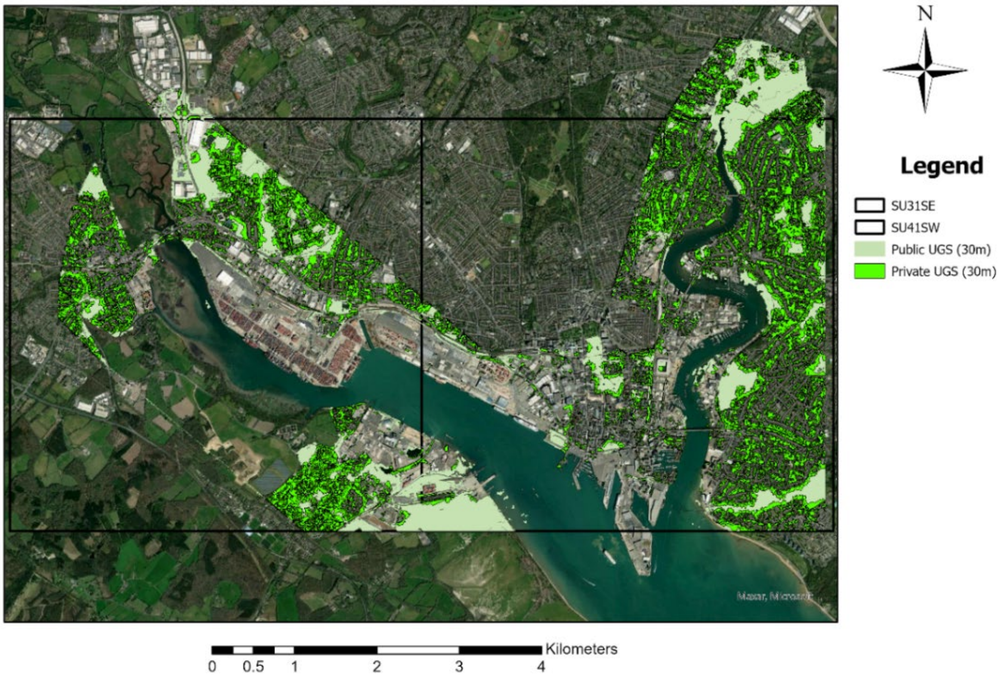

Figure 4.16 Private and public UGS distributions calculated with different threshold distances (highest accuracy (top), determined threshold 30m (down))

It has been calculated that there are 17975 trees in the study area. There are approximately 528 trees per square kilometre. In Figure 4.17, the number of trees in 1km^2 grids is shown. Especially in the port and industrial area, the tree density is very low compared to other regions. The density of trees is higher in the northeast of the study area compared to other regions. Covering only 3.97% of the study area, SU4315 and SU4415 grids have 1986 trees. This corresponds to 11% of the total number of trees in this 1.35 km^2 area.

Figure 4.17 Tree density map

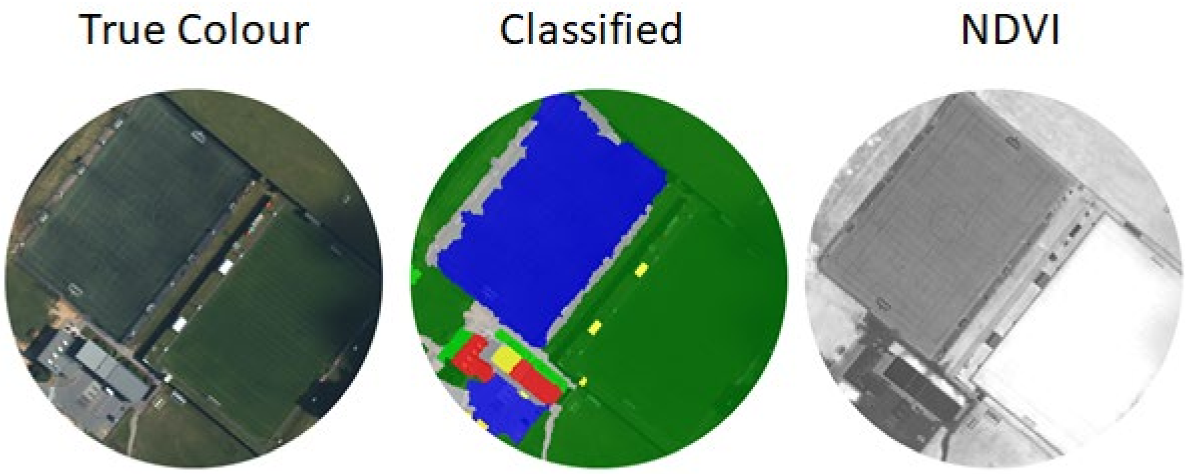

Figure 4.18 True colour, classified and NDVI image of an artificial Green

The green spaces in the study area are not only vegetation. As seen in Figure 4.18, although two football pitches side by side are similar in shape and colour, one is natural vegetation while the other is artificial. Therefore, the natural grass field on the right, which has chlorophyll pigments, has an average NDVI value of 0.57, while the NDVI value of the artificial grass pitch on the left is approximately -0.08.

5. DISCUSSION

This chapter aims to evaluate of methods applied in this study to get results with critical analyses, limitations of data and methods also suggestions for future studies.

Data pre-processing, segmentation, object-based classification, and methods of green space analysis will be discussed separately in each section respectively. In section 5.5 limitations of the study will be explained, and suggestions for future studies will make in section 5.6.

5.1. Data Pre-processing

When mosaicking aerial images and DEMs, two different methods have been applied. Nearest neighbour for aerial images and bilinear interpolation for DEM. The reason is that when using the nearest neighbour method, the original DN values of aerial image is kept due to data processing time increasing caused by data size. Although this geometric correction process has speed and not alter the DN values advantages, can cause duplication and loss of some pixels (Baboo and Devi, 2010). However, vertical aerial photographs have little geometric distortions (Weng, 2012).

On the other hand, the DEM data was resampled by using the bilinear method. This method has been chosen to preserve the continuous structure of the data, even if the pixel values change due to the production of new pixel values by taking the weighted average of four neighbouring pixel values even though the contrast and sharpness quality of some pixels may decrease (Thurnhofer and Mitra, 1996).

After the mosaicking process, geometric correction was continued for produced nDSMs and aerial images as setting the place of images in space as defining the coordinate systems. However, some geometric distortions can be caused by the curvature and rotation of the Earth, errors of simultaneous GPS/IMU navigation, atmospheric refraction, and change of the speed of the vehicle taken image (Toutin, 2004). These distortions may only partially be eliminated, which is one reason for misclassification.

Figure 4.4 shows the atmospheric distortion and misclassification that it causes. In the image, the straight line of the bridge has been distorted by the effect of one or more of the sources of atmospheric distortion, and as a result, some areas, and parts of the vegetation are misclassified.

Because of the heterogenic structure of the atmosphere, gas particles, water vapour, and clouds affect the signals from the airborne vehicle and cause atmospheric distortions (Song et al., 2001). In this study, also atmospheric distortions affect the accuracy of classifications. For instance, the cloud covers an approximately 520 m long 370 m wide area. Because the image taken by the camera did not detect the land's surface or object, this object caused some water, residential areas, and green space to be misclassified as non-residential areas (Figure 4.5).

Atmospheric errors do not only consist of the cloud view in the image, but it also causes blurriness because of the angle of illumination from the Sun, and this effect is higher in the summertime. The vertical aerial photographs taken in August 2019 have this distortion as well. However, images could be atmospherically corrected using radiative transfer models or by eliminating data with near-zero reflectance values using the dark object subtraction method. (Black et al., 2014; Chavez, 1988). Nevertheless, it can get higher accuracy by using an atmospherically corrected image than a not corrected one; however, the accuracies are not remarkably different (Siregar et al., 2018).

5.2. Segmentation

Segments are units to be classified in OBIA, these can only be assigned to a class, and the segmentation step is considered the most important step of object-based classification (Belgiu and Drăgut, 2014; Burnett and Blaschke, 2003). For this reason, segmentation has seriously affected the classification accuracy and, therefore, the accuracy of the separation of public and private green spaces and tree density. The accuracy of subsequent OBIA is primarily determined by image segmentation quality (Su and Zhang, 2017). The average size of the segments notably affects the classification accuracy (Gao et al., 2011). The main reason the 1m resolution data classification is less accurate than other classifications is that the same image object contains different class objects (Table 4.1). For example, the green areas around most of the dwellings in the test area (Figure 3.11) were segmented as the same image object and, as a result, were mostly classified as trees (Figure 4.2).

The pixel of 1 m resolution image represents an area 25 times the size of a pixel in the 0.2 m resolution image, which means spectral and spatial precision of coarser resolution image is lower. Because of this situation, 1 m resolution data segmentation is less accurate. In the MRS algorithm, pixels form image objects by grouping them according to the similarity of their texture, density, and shape (Wei et al., 2005). Consequently, the area corresponding to different entities in coarser resolution images was segmented as a single image object.

In addition, none of the entities belonging to the same LULC class can be of the same size, shape, or spectral feature as the other. For example, the roof of each residential building can be a different colour and shape (Figures 3.8 and 3.11), although all of it should be classified as a residential area. Therefore, it is challenging to accurately represent real objects by forming the pixels that make the image into objects with SP, shape, and compactness parameters. However, choosing of an accurate SP value is a critical decision in remote sensing imagery segmentation (Kim et al., 2011). Consequently, in this research Drăguţ et al. (2014) using the automatic SP estimation tool, it is aimed to keep the segmentation as far from subjectivity as possible. Nevertheless, this tool estimates different SP for different weights of shape and compactness; therefore, the selection of image objects is not independent of subjectivity.

If there was no time limitation to segment the study area, the study area could be chosen for using ESP-2 tool to segment instead of segmentation test areas (Figures 3.4 and 3.5). In this way, more accurate SP, shape, and compactness parameters would have been determined for the entire study area. Therefore, more meaningful image objects could be obtained result of MSR. However, as in this study, it is ideal to apply the same SP value in segmentation for images with the same resolution, especially if one is a subset of the other, because the most decisive factor for estimating SP value is the resolution of the image (Möller et al., 2007).

5.3. Object-based Image Classification

In this study, it was possible to compare the classification methods and the results by applying different images, methods, and rulesets. There are many parameters that affect classification accuracy. Only vertical aerial photograph data were used when selecting training samples while supervised classification carried out. Coverage and spectral variation of the training samples affected the quality of OBIA (Li et al., 2016). Also, the selection of samples in nearest neighbour supervised classification is a crucial step that could decrease the complexity of classification by eliminating unnecessary features for classification (Ma et al., 2017a). However, supervised OBIA classification has some disadvantages compared to the rule-based approach. These area mainly, how training samples of homogeneous classes will better represent complex objects of same classes, and the issue of which objects will produce more accurate results when selected training samples according to the complexity of the objects are still uncertain also the subjectivity of training selection brings other uncertainties (Dronova et al., 2011; Ma et al., 2017b).

In supervised and rule-based OBIA, a segment is the smallest unit of classification, which is grouped into pixels as a meaningful object. However, it is more complex than a single pixel, and a better alternative to the pixel-based method by eliminating the artificial square cell problem in the pixel-based method, especially in high-resolution images (Burnett and Blaschke, 2003). However, despite all the advantages that OBIA brings to image classification, the visual dynamics of objects and the relationship with their environment is a matter that cannot be observed via pixels or image objects because pixels are just an optical output unit of sensed radiation, which is represented as digital numbers. For this reason, OBIA is not yet a technology that can distinguish objects from each other with complete accuracy. Moreover, higher spatial resolution does not always mean higher accuracy in object-based classification (Powers et al., 2012).

In addition, the positions of the bands in the electromagnetic spectrum also affect the classification. 0.2 m resolution data consists of 4 bands, and the bands are defined by the manufacturer as red, green, blue and NIR. However, 1 m resolution CASI multispectral data consists of 22 spectral bands, and one colour corresponds to more than one band. In general, Blue 450-480 nm, green 510-550 nm, red 550-700 nm, and NIR 750-2500 nm are wavelength ranges (Gitelson and Merzlyak, 1998; Walsh et al., 2020; Wang et al., 2011). Moreover, in CASI multispectral data, especially the red and NIR colours correspond to more than one band (Table 3.4). Selecting different bands changes the DN value of a pixel and, as a result, DN values of image objects which are consisting of pixels. This situation would lead to different results in the NDVI, NDWI and brightness values used in the classification. Therefore, using different bands can change the LULC classes of all objects, especially water, trees, grassland and non-residential.

Besides, especially shadow density caused by the building's heights caused misclassification (Figure 4.6). Shadows that are part of the same image object as dwellings, not roads, are classified as residential area. On the other hand, the applied segmentation process successfully separated different objects into different segments. The determined ruleset-2 worked well to separate classes from the buildings around the green spaces (Figure 4.6). Nevertheless, various alternatives could be used when determining threshold values, for example the automatic induction and cognitive method (Lloyd et al., 2002; Tullis and Jensen, 2003) or FODPSO algorithm developed by Ghamisi et al. (2012). Also as in this study, thresholds based on image object information determined by users can be used (Hodgson et al., 2003). By using NDVI and NDWI indices, it has been tried to differentiate objects from water and vegetation. However, it is very difficult task to distinguish urban LULC types each other (Shackelford and Davis, 2003). For example, in the port region, containers are of various colours and often have similar spectral characteristics to building roofs. Therefore, many containers are classified as residential areas (Figure 4.7). However, the solution of such limitations is not possible, and they cause misclassification. There is plenty of spectral differences in even one LULC class. For example, roofs of residential buildings can be in different colours or non-residential areas consist of many structures different colour and shape. Therefore, no matter how high the resolution of the image in areas containing natural and artificial presence with very different characteristics from each other, a high-accuracy result may not be achieved using object-based classification. Moreover, there are many non-permanent mobile objects in cities. For example, boats on the river have caused areas that are water to be classified as road (Figure 4.8). However, if some of these boats were segmented together with water as the same image object, they would be classified as water as the threshold values determined in the ruleset classify the objects according to the average values of the pixels that units of the segments, which is more likely in lower resolution images.

The accuracy rates of classifications depend on many parameters. Some misclassifications can be noticed with visually interpretation, but numerical accuracy should be evaluated using reference data to determine the accuracy of the LULC map produced and subsequent studies based on this data.

Accuracy assessment approaches in object-based classification are of two types, per-pixel, and per-polygon approach, according to the agreement unit (Stehman and Wickham, 2011). In this study, the accuracy assessment was carried out with both approaches. The per-pixel method, which is preferred when calculating the overall accuracy and kappa values of the LULC maps. Depending on the distribution and number of randomly produced reference points the different overall accuracy and kappa coefficient values could be achieved, and this approach produced a relatively inconsistent result. Therefore, the per-polygon method was preferred in the calculation of the urban green space distribution although per-pixel approach is more common used (Powers et al., 2012). However, evaluating the extent to which the classified objects overlap with the area corresponding to that object gives more appropriate results about the accuracy of the study compared to the pixel-based accuracy assessment (Ma et al., 2017b). With this approach, reference polygons and classified vegetation and residential area polygons were compared on an area basis and TPR, FPR and accuracy ratios were calculated (Tables 4.2, 4.3

and 4.4). Therefore, the accuracy analysis of the data to be used in private, public UGS and tree density studies has been carried out with more precision.

5.4. Green Space Detection

Separation of the public and private UGS and tree density were calculated with information from object-based classification result. Therefore, the factors that affect the quality of the classification are crucial in the accuracy of the green space distribution. However, the reasons be based on the vegetation structure also affected the result.

In this study, the height data is the only parameter used to distinguish between trees and grassland. This has advantages and disadvantages in getting precise results. Since the tree crowns are not flat but hollow, there are gaps between leaves; therefore, the LiDAR pulses to contact the ground directly or the trunk of the trees without reaching the tree crown. Therefore, in DSM generated from the first return LiDAR point cloud data, trees can be represented differently from their crown height. Consequently, some trees were misclassified as grassland (Figure 4.9).

Nevertheless, objects were classified as tree or grassland according to their mean height values (nDSM). Despite, even if some LiDAR data represents the ground height, the average of the pixels of the segment also includes the height information of the pulses contacting the tree crown. For this reason, a relatively low threshold value (0.6 m) was chosen for separating trees and grassland, relative to a tree height. Moreover, tree crowns are classified with higher accuracy in condition that they are segmented with high precision as image objects separate from grasslands because of their spectral and especially spatial properties (Fisher et al., 2020). In addition, tree crowns can be detected and delineated individually by choosing tree crown samples from the combination of LiDAR data and aerial images (Zhen et al., 2016). This approach relying on the trees which are represented by bright pixels in DEM data and bounded by low density pixels in shadow or less bright parts of the tree crown (Leckie et al., 2003).

Nonetheless, classifying the tree crowns in urban is challenging process because of the diversities of canopies in urban, also composition of the cities where trees and other objects exist together even in a small area (Salim et al., 2018). In addition, using height information to detect canopies is not an adequate approach to get satisfactory results in urban areas, because in cities are likely to exist higher features than canopy structures. In this case, using only nDSM data might not be preferred for tree detection because height information does not enough to separate trees from other relatively higher objects (Sung, 2012). Furthermore, trees are not only be distinguished using height information but also, they can be detected according to their spectral and spatial properties. Therefore, using geometric values of image objects, such as elliptic fit, the ratio of length and width and roundness as threshold when deciding the ruleset, could be perform better for separating trees from other urban features (Ardila et al., 2012). Also, because the tree crown sizes are different from one, using the OBIA approach for individual tree crown detection (ITCD) results in either some trees being detected as over-segmented or multiple trees as a single segment. (Jakubowski et al., 2013).

To the extent that trees can be distinguished correctly, grasslands can be classified correctly in this study. Additionally, the use of the NDVI index may not always give very high accuracy in separating vegetation (Sun and Meng, 2020). However, the UGS existence was determined by using NDVI and height information in this study. Therefore, accuracies of public and private UGS and tree density calculations are based upon NDVI and height information performances of detecting trees and grassland.

5.5. Limitations

Limitations stem from the methodology followed to make a classification in this study have already been discussed in this chapter. However, the limitations are not limited to these. There are also constraints of the data and software used because of the definitions of public and private green spaces.

A spatial assessment of the UGS in Southampton requires remotely sensed data covering the entire city. However, out of the six grid tiles covering Southampton, only about 34 km^2 data of the 150 km^2 area is available in Environment Agency database. Therefore, only in an area of this size could Southampton be geospatially evaluated in terms of green spaces with these data. Nevertheless, the size of even these available data is enormous. For example, the size of 2019 vertical aerial photographs and 2018 nDSM data processed together is 19.4 GB and therefore a segmentation operation took hours.

The object-based classification was carried out in licensed software, eCognition Developer 9. There are time and data processing limitations as this software is available on a limited number of computers, which are only accessible at certain times of the day.

In line with the aim of the study, it is critical to detect green areas with high accuracy. Since the LiDAR data used in the study was produced with a +/- 15 cm root-mean-square error affects the accuracy of the tree classifications made using the height data. Since nDSM data is produced using DSM and DTM data together, the cumulative vertical error can reach +/- 30 cm. Therefore, the results produced using the height data in the study can only be calculated within this accuracy.

The classification results used in the green space analyses were produced by using vertical aerial photograph and DEM data together. These were achieved not simultaneously by the producer. LiDAR point data from which DEM was produced were obtained with flights in February 2018, and vertical aerial photographs were obtained with flights in August 2019. Earth objects may have different spatial and spectral properties at different times. This can cause different objects to be detected at the same location in this data. Furthermore, the data were obtained at different times of the year. Due to phenological effects, both geometric and colour properties of plants differ from each other in February and August. This situation leads to the conclusion that the height of a tree that has already lost its leaves in February, when DEM data is taken, cannot be determined well by airborne measurement technique. Also, at these times of the year, the colour of the vegetation differs from each other, except evergreen vegetation species (Dong et al., 2015). Additionally, because of the lack of open-source data of actual tree locations, an accuracy assessment of tree location could not be carried out.

There are also constraints in the detection of buildings. Airborne remotely sensed data is insufficient in determining whether a building is a residential area because the roof of these buildings can be of different colours and shapes. Moreover, buildings with the same characteristics can be non-residential or residential. However, the way to distinguish private and public green spaces requires classifying dwellings separately from non-residential spaces.

In addition, whatever value threshold distance is chosen, the proximity approach is not adequate to distinguish whether a UGS is private or public. The main reason for this is that private domestic gardens have no size limit. The border of a private UGS can reach much further distances than the building it belongs to. Furthermore, determining whether a UGS is private or public is a matter of property law. Therefore, no matter which geospatial analysis approach is preferred, green areas cannot be classified with full accuracy as public or private without ownership information.

5.6. Direction of Future Research

By removing the evaluated constraints as much as possible, new approaches can be taken to the study. Consequently, a range of studies can be developed on this subject.

Available data do not cover a significant portion of Southampton. No Environment Agency LiDAR or VHR data is available covering Southampton's largest open green space, Southampton Common, with an area of approximately 1.48 km^2. Also, the production frequency of LiDAR data is annual and aerial images are in every 6 and 7 years. If the frequency of production and coverage of the data are increased, geospatial analysis of UGS in Southampton can be done more comprehensively. Nonetheless, open-source VHR data are available for some part of Southampton, however VHR data may not be available covering the study area of future studies of the same purpose. As access to higher resolution data increases, UGS studies will gain a new dimension.

Recent circumstances have revealed that remote sensing approaches to green area detection need to be developed. Although not unlike a visually green space, non-living "fake grass" (Figure 4.18) has recently become a prevalent phenomenon in private green spaces in the UK (Newlone, 2022). These green areas, where the vegetation indices are insufficient to detect, might be the subject of future UGS studies.

In addition, the threshold distance value determined, to separate public and private green areas, was decided as a result of the accuracy analysis carried out using the reference data produced by the Ordnance Survey. However, this kind of reference data for every country is not available. Nevertheless, private and public green space datasets can be created for different countries by applying the methodology followed in this study. Besides, combining the population data with this study outcomes can be used to calculate how far different types of UGS are from people and how accessible they are.

ESP-2 tool developed by Drăguţ et al. (2014) tool makes scale estimation for a single shape and compactness parameters in one time. If the tool will develop that can estimate one SP value considering for all shape and compactness parameters possibilities, it will increase the segmentation accuracy in future studies.

The eCognition is a paid software designed for object-based image classification. For becoming widespread of OBIA studies, freely accessible alternatives such as the object-based image analysis tool of the Google Earth Engine platform can be developed, or new freely accessible alternatives can be produced.

6. CONCLUSION

In conclusion, the distribution of public and private green space and tree density in Southampton were calculated using the Environment Agency available LiDAR and very high-resolution data in this study. In the object-based classification results performed to decide the most suitable OBIA method for this aim.

The lowest overall accuracy and kappa value of 40% and 0.29 are the result of classification using 1 m spatial resolution 2013 CASI multispectral image and 2014 DEM data. As a result of the classification of the test area of 0.2 m resolution 2019 vertical aerial photographs and 2018 DEM data using the threshold values expressed as "ruleset-2" in the study, the highest accuracy values were found as 82% overall accuracy and 0.78 kappa. Using the "ruleset-2" values, the study area was classified with an overall accuracy of 72% and an accuracy of 0.66 kappa.

With the consequence data of this classification, UGS in Southampton were classified as private and public, and the green area distribution of the city was calculated, also tree density in the city mapped. The number of trees per square kilometre in the study area was calculated as 528.

It has been calculated that the green areas in the study area are approximately equally distributed in all directions of the areas classified as residential areas. In addition, according to all threshold distance decided in this study, the private green space is more than the public green space in Southampton. As the threshold distance values increased which was selected for the classification of public and private UGS, the accuracy value of private green spaces decreased, while the accuracy value of public green spaces increased. When the green areas at a maximum distance of 10 m from the dwellings are accepted as private UGS, the highest private UGS accuracy was found as 46.5%. When the UGS at least 40 m away from the residential buildings are accepted as public green space, the highest public green space accuracy was obtained with 39.1%.

SU31SE and SU41SW grids, which constitute more than 95% of the area of the study, were compared in terms of green area distribution. Sum of private and public green spaces in SU31SE is 3.86 km^2. The total amount of public and private green spaces in SU41SW grid tile is 5.31 km^2. Private green space in the SU41SW grid is 68.9% of total UGS. In the SU31SE, 66.8% of the total UGS is private.

Considering that Port of Southampton and other industrial regions around it covers a significant part of the study area, it can be said that Southampton is a relatively green city based on the green space and tree density calculated. To benefit from the environmental, health and socioeconomical benefits of these areas and to pass them to the future generations, it is necessary to protect the green areas in the city effectively and to progress their spatial analyses based on well-designed plans, like "Southampton Greener City Plan 2030".

7. REFERENCES

Ahern, J., 2011. From fail-safe to safe-to-fail: Sustainability and resilience in the new urban world. *Landscape and urban Planning*, *100*(4), pp.341-343.

Almanza, E., Jerrett, M., Dunton, G., Seto, E. and Pentz, M.A., 2012. A study of community design, greenness, and physical activity in children using satellite, GPS and accelerometer data. *Health & place*, *18*(1), pp.46-54.

Andrusaityte, S., Grazuleviciene, R., Dedele, A. and Balseviciene, B., 2020. The effect of residential greenness and city park visiting habits on preschool Children's mental and general health in Lithuania: A cross-sectional study. *International Journal of Hygiene and Environmental Health*, *223*(1), pp.142-150.

Ardila, J.P., Bijker, W., Tolpekin, V.A. and Stein, A., 2012. Context-sensitive extraction of tree crown objects in urban areas using VHR satellite images. *International journal of applied earth observation and geoinformation*, *15*, pp.57-69.

Armson, D., Stringer, P. and Ennos, A.R., 2012. The effect of tree shade and grass on surface and globe temperatures in an urban area. *Urban Forestry & Urban Greening*, *11*(3), pp.245-255.

Asmaryan, S., Warner, T.A., Muradyan, V. and Nersisyan, G., 2013. Mapping tree stress associated with urban pollution using the WorldView-2 Red Edge band. *Remote Sensing Letters*, *4*(2), pp.200-209.

Astell-Burt, T. and Feng, X., 2019. Association of urban green space with mental health and general health among adults in Australia. *JAMA network open*, *2*(7), pp.e198209-e198209.

Baatz, M., 2000. Multi resolution segmentation: an optimum approach for high quality multi scale image segmentation. In *Beutrage zum AGIT-Symposium. Salzburg, Heidelberg, 2000* (pp. 12-23).

Baboo, S.S. and Devi, M.R., 2010. An analysis of different resampling methods in Coimbatore, District. *Global Journal of Computer Science and Technology*.

Bassett, R., Cai, X., Chapman, L., Heaviside, C., Thornes, J.E., Muller, C.L., Young, D.T. and Warren, E.L., 2016. Observations of urban heat island advection from a high-density monitoring network. *Quarterly Journal of the Royal Meteorological Society*, *142*(699), pp.2434-2441.

Belgiu, M. and Drăguţ, L., 2014. Comparing supervised and unsupervised multiresolution segmentation approaches for extracting buildings from very high-resolution imagery. *ISPRS Journal of Photogrammetry and Remote Sensing*, *96*, pp.67-75.

Bilgili, B.C. and Gökyer, E., 2012. Urban green space system planning. *Landscape planning*, 360.

Black, M., Fleming, A., Riley, T., Ferrier, G., Fretwell, P., McFee, J., Achal, S. and Diaz, A.U., 2014. On the atmospheric correction of antarctic airborne hyperspectral data. *Remote Sensing*, *6*(5), pp.4498-4514.

Blaschke, T., Hay, G.J., Kelly, M., Lang, S., Hofmann, P., Addink, E., Feitosa, R.Q., Van der Meer, F., Van der Werff, H., Van Coillie, F. and Tiede, D., 2014. Geographic object-based image analysis–towards a new paradigm. *ISPRS journal of photogrammetry and remote sensing*, *87*, pp.180-191.

Blaschke, T., Lang, S. and Hay, G. eds., 2008. *Object-based image analysis: spatial concepts for knowledge-driven remote sensing applications*. Springer Science & Business Media.

Borenstein, E. and Ullman, S., 2008. Combined top-down/bottom-up segmentation. *IEEE Transactions on pattern analysis and machine intelligence*, *30*(12), pp.2109-2125.

Boulton, C., Dedekorkut-Howes, A. and Byrne, J., 2018. Factors shaping urban green space provision: A systematic review of the literature. *Landscape and urban planning*, *178*, pp.82-101.

Bradley, C.A. and Altizer, S., 2007. Urbanization and the ecology of wildlife diseases. *Trends in ecology & evolution*, *22*(2), pp.95-102.

Bren d'Amour, C., Reitsma, F., Baiocchi, G., Barthel, S., Güneralp, B., Erb, K.H., Haberl, H., Creutzig, F. and Seto, K.C., 2017. Future urban land expansion and implications for global croplands. *Proceedings of the National Academy of Sciences*, 114(34), pp.8939-8944.

Burnett, C. and Blaschke, T., 2003. A multi-scale segmentation/object relationship modelling methodology for landscape analysis. *Ecological modelling*, *168*(3), pp.233-249.

Caynes, R.J., Mitchell, M.G., Wu, D.S., Johansen, K. and Rhodes, J.R., 2016. Using high-resolution LiDAR data to quantify the three-dimensional structure of vegetation in urban green space. *Urban ecosystems*, *19*(4), pp.1749-1765.

Chavez Jr, P.S., 1988. An improved dark-object subtraction technique for atmospheric scattering correction of multispectral data. *Remote sensing of environment*, *24*(3), pp.459-479.

Chen, W., Huang, H., Dong, J., Zhang, Y., Tian, Y. and Yang, Z., 2018. Social functional mapping of urban green space using remote sensing and social sensing data. *ISPRS Journal of Photogrammetry and Remote Sensing*, *146*, pp.436-452.

Cheng, L., Chen, S., Chu, S., Li, S., Yuan, Y., Wang, Y. and Li, M., 2017. LiDAR-based three-dimensional street landscape indices for urban habitability. *Earth Science Informatics*, *10*(4), pp.457-470.

Chuai, X.W., Huang, X.J., Wang, W.J. and Bao, G., 2013. NDVI, temperature and precipitation changes and their relationships with different vegetation types during 1998–2007 in Inner Mongolia, China. *International journal of climatology*, 33(7), pp.1696-1706.

Chunyan, Z.H.U., Wenping, R.E.N., Yifeng, Y.I.N., Wenhan, X.I.E. and Weidong, L.I.U., 2016. The Planning of Green spaces to Prevent and Avoid Urban Disasters in Dujiangyan. *International Journal of Simulation--Systems, Science & Technology*, *17*(46).

Clark, P., Niemi, M. and Nolin, C. eds., 2017. *Green landscapes in the European city, 1750-2010*. Routledge.

Collins, R.M., Spake, R., Brown, K.A., Ogutu, B.O., Smith, D. and Eigenbrod, F., 2020. A systematic map of research exploring the effect of green space on mental health. *Landscape and Urban Planning*, *201*, p.103823.

ConservatoryLand, 2021. *Biggest Garden Capitals in the UK*. [Online]. [Accessed 06 July 2022]. Available from: https://www.conservatoryland.com/blog/biggest-garden-capitals-in-the-uk/

Coolen, H. and Meesters, J., 2012. Private and public green spaces: meaningful but different settings. *Journal of Housing and the Built Environment*, *27*(1), pp.49-67.

Corley, J., Okely, J.A., Taylor, A.M., Page, D., Welstead, M., Skarabela, B., Redmond, P., Cox, S.R. and Russ, T.C., 2021. Home garden use during COVID-19: Associations with physical and mental wellbeing in older adults. *Journal of environmental psychology*, *73*, p.101545.

Darcy, P.M., Taylor, J., Mackay, L., Ellis, N.J. and Gidlow, C.J., 2022. Understanding the Role of Nature Engagement in Supporting Health and Wellbeing during COVID-19. *International journal of environmental research and public health*, *19*(7), p.3908.

Definiens, A.G., 2007. eCognition user guide.

DEFRA, 2021. *Rural population and migration*. [Online]. [Accessed 02 July 2022]. Available from: https://www.gov.uk/government/statistics/rural-population-and-migration/rural-population-and-migration

Dennis, M. and James, P., 2017. Evaluating the relative influence on population health of domestic gardens and green space along a rural-urban gradient. *Landscape and Urban Planning*, *157*, pp.343-351.

Dieleman, F. and Wegener, M., 2004. Compact city and urban sprawl. *Built environment*, *30*(4), pp.308-323.

Dong, J., Xiao, X., Kou, W., Qin, Y., Zhang, G., Li, L., Jin, C., Zhou, Y., Wang, J., Biradar, C. and Liu, J., 2015. Tracking the dynamics of paddy rice planting area in 1986–2010 through time series Landsat images and phenology-based algorithms. *Remote Sensing of Environment*, *160*, pp.99-113.

Drăguţ, L., Csillik, O., Eisank, C. and Tiede, D., 2014. Automated parameterisation for multi-scale image segmentation on multiple layers. *ISPRS Journal of photogrammetry and Remote Sensing*, *88*, pp.119-127.

Dronova, I., Gong, P. and Wang, L., 2011. Object-based analysis and change detection of major wetland cover types and their classification uncertainty during the low water period at Poyang Lake, China. *Remote sensing of Environment*, *115*(12), pp.3220-3236.

eCognition Developer, T., 2014. 9.0 User Guide. Trimble Germany GmbH: Munich, Germany.

Environment Agency (no date). *LIDAR Home*. ArcGIS Experience Builder. [Online]. [Accessed: 20 July 2022]. Available from: https://experience.arcgis.com/experience/753ad2ebd3554fa696885b8c366c3049/page/LIDAR/

Environment Agency CASI Multispectral Imageries [Geospatial Data], Tile(s): SU31NE, SU31SE, SU41NW, SU41SW, SU41NE, SU41SE, Environment Agency, 2013, Using: DEFRA Data

Services Platform. [Online]. [Accessed: 04 July 2022]. Available from: https://environment.data.gov.uk/DefraDataDownload/?Mode=survey

Environment Agency LiDAR Tiles DSM [Geospatial Data], Tile(s): SU31NE, SU31SE, SU41NW, SU41SW, SU41NE, SU41SE, Environment Agency, 2014, Using: DEFRA Data Services Platform. [Online]. [Accessed: 04 July 2022]. Available from: https://environment.data.gov.uk/DefraDataDownload/?Mode=survey

Environment Agency LiDAR Tiles DTM [Geospatial Data], Tile(s): SU31NE, SU31SE, SU41NW, SU41SW, SU41NE, SU41SE, Environment Agency, 2018, Using: DEFRA Data Services Platform. [Online]. [Accessed: 04 July 2022]. Available from: https://environment.data.gov.uk/DefraDataDownload/?Mode=survey

Environment Agency Vertical Aerial Photographs [Geospatial Data], Tile(s): SU31NE, SU31SE, SU41NW, SU41SW, SU41NE, SU41SE, Environment Agency, 2019, Using: DEFRA Data Services Platform. [Online]. [Accessed: 04 July 2022]. Available from: https://environment.data.gov.uk/DefraDataDownload/?Mode=survey

European Commission, 2012. *Urban Atlas Mapping Guide* [Online]. [Accessed: 27 August 2022]. Available from: https://land.copernicus.eu/user-corner/technical-library/urban-atlas-mapping-guide

European Commission, 2013. *Communication From The Commission To The European Parliament, The Council, The European Economic And Social Committee And The Committee Of The Regions* [Online]. [Accessed: 27 August 2022] Available from: https://eur-lex.europa.eu/resource.html?uri=cellar:d41348f2-01d5-4abe-b817-4c73e6f1b2df.0014.03/DOC_1&format=PDF

Fisher, A., Armston, J., Goodwin, N. and Scarth, P., 2020. Modelling canopy gap probability, foliage projective cover and crown projective cover from airborne lidar metrics in Australian forests and woodlands. *Remote Sensing of Environment*, *237*, p.111520

Franco, S.F. and Macdonald, J.L., 2018. Measurement and valuation of urban greenness: Remote sensing and hedonic applications to Lisbon, Portugal. *Regional Science and Urban Economics*, *72*, pp.156-180.

Gao, B.C., 1996. NDWI—A normalized difference water index for remote sensing of vegetation liquid water from space. *Remote sensing of environment*, 58(3), pp.257-266.

Gao, Y.A.N., Mas, J.F., Kerle, N. and Navarrete Pacheco, J.A., 2011. Optimal region growing segmentation and its effect on classification accuracy. *International journal of remote sensing*, *32*(13), pp.3747-3763

Gascon, M., Triguero-Mas, M., Martínez, D., Dadvand, P., Rojas-Rueda, D., Plasència, A. and Nieuwenhuijsen, M.J., 2016. Residential green spaces and mortality: a systematic review. *Environment international*, 86, pp.60-67.

Gaston, K.J., Warren, P.H., Thompson, K. and Smith, R.M., 2005. Urban domestic gardens (IV): the extent of the resource and its associated features. *Biodiversity & Conservation*, 14(14), pp.3327-3349.

Ghamisi, P., Couceiro, M.S., Benediktsson, J.A. and Ferreira, N.M., 2012. An efficient method for segmentation of images based on fractional calculus and natural selection. *Expert Systems with Applications*, *39*(16), pp.12407-12417.

Gitelson, A.A. and Merzlyak, M.N., 1998. Remote sensing of chlorophyll concentration in higher plant leaves. *Advances in Space Research*, *22*(5), pp.689-692.

Goddard, M.A., Dougill, A.J. and Benton, T.G., 2010. Scaling up from gardens: biodiversity conservation in urban environments. *Trends in ecology & evolution*, 25(2), pp.90-98.

Gülçin, D. and AKPINAR, A., 2018. Mapping Urban Green spaces Based on an Object-Oriented Approach. *Bilge International Journal of Science and Technology Research*, *2*, pp.71-81.

Haara, A. and Haarala, M., 2002. Tree species classification using semi-automatic delineation of trees on aerial images. *Scandinavian Journal of Forest Research*, *17*(6), pp.556-565.

Harrison, A R., 2006. National Land Use Database: Land Use and Land Cover version 4.4. Office of the Deputy Prime Minister. [Online]. [Accessed: 21 July 2022]. Available from: https://www.gov.uk/government/statistics/national-land-use-database-land-use-and-land-cover-classification

Havinga, I., Bogaart, P.W., Hein, L. and Tuia, D., 2020. Defining and spatially modelling cultural ecosystem services using crowdsourced data. *Ecosystem Services*, 43, p.101091.

Heidt, V. and Neef, M., 2008. Benefits of urban green space for improving urban climate. In *Ecology, planning, and management of urban forests* (pp. 84-96). Springer, New York, NY.

Hettiarachchi, T. and Wijesundara, C.S., 2017. Conservational significance of Dunumadalawa Forest Reserve in Central Sri Lanka based on the endemism of its avifauna. *Ceylon Journal of Science*, *46*(3), pp.21-30.

Hodgson, M.E., Jensen, J.R., Tullis, J.A., Riordan, K.D. and Archer, C.M., 2003. Synergistic use of lidar and color aerial photography for mapping urban parcel imperviousness. *Photogrammetric Engineering & Remote Sensing*, *69*(9), pp.973-980.

Hoffimann, E., Barros, H. and Ribeiro, A.I., 2017. Socioeconomic inequalities in green space quality and accessibility—Evidence from a Southern European city. *International journal of environmental research and public health*, 14(8), p.916.

Huang, Y., Yu, B., Zhou, J., Hu, C., Tan, W., Hu, Z. and Wu, J., 2013. Toward automatic estimation of urban green volume using airborne LiDAR data and high-resolution remote sensing images. *Frontiers of Earth Science*, *7*(1), pp.43-54.

Huerta, R.E., Yépez, F.D., Lozano-García, D.F., Guerra Cobián, V.H., Ferriño Fierro, A.L., de León Gómez, H., Cavazos González, R.A. and Vargas-Martínez, A., 2021. Mapping Urban Green spaces at the Metropolitan Level Using Very High-resolution Satellite Imagery and Deep Learning Techniques for Semantic Segmentation. *Remote Sensing*, 13(11), p.2031.

Jakubowski, M.K., Li, W., Guo, Q. and Kelly, M., 2013. Delineating individual trees from LiDAR data: A comparison of vector-and raster-based segmentation approaches. *Remote Sensing*, *5*(9), pp.4163-4186.)

Jensen, R., Gatrell, J., Boulton, J. and Harper, B., 2004. Using remote sensing and geographic information systems to study urban quality of life and urban forest amenities. *Ecology and Society*, *9*(5).

Jeong, S. and Yoon, D.K., 2018. Examining vulnerability factors to natural disasters with a spatial autoregressive model: The case of South Korea. *Sustainability*, 10(5), p.1651.

Jim, C.Y., 1989. Tree canopy cover, land use and planning implications in urban Hong Kong. *Geoforum*, *20*(1), pp.57-68.

Khatriker, S. and Kumar, M., 2018. Building footprint extraction from high-resolution satellite imagery using segmentation. *The International Archives of Photogrammetry, Remote Sensing and Spatial Information Sciences*, *42*, pp.123-128.

Kim, H., Lee, D.K. and Sung, S., 2016. Effect of urban green spaces and flooded area type on flooding probability. *Sustainability*, *8*(2), p.134.

Kim, M., Warner, T.A., Madden, M. and Atkinson, D.S., 2011. Multi-scale GEOBIA with very high spatial resolution digital aerial imagery: scale, texture and image objects. *International Journal of Remote Sensing*, *32*(10), pp.2825-2850.

Kwan, C., Gribben, D., Ayhan, B., Li, J., Bernabe, S. and Plaza, A., 2020. An accurate vegetation and non-vegetation differentiation approach based on land cover classification. *Remote Sensing*, *12*(23), p.3880.

Lachowycz, K. and Jones, A.P., 2011. Green space and obesity: a systematic review of the evidence. *Obesity reviews*, 12(5), pp.e183-e189.

Laliberte, A.S. and Rango, A., 2009. Texture and scale in object-based analysis of subdecimeter resolution unmanned aerial vehicle (UAV) imagery. *IEEE Transactions on Geoscience and Remote Sensing*, *47*(3), pp.761-770.

Landis, J.R. and Koch, G.G., 1977. The measurement of observer agreement for categorical data. *biometrics*, pp.159-174.

Lang, S., Schöpfer, E., Hölbling, D., Blaschke, T., Moeller, M., Jekel, T. and Kloyber, E., 2008. Quantifying and qualifying urban green by integrating remote sensing, GIS, and social science method. In *Use of landscape sciences for the assessment of environmental security* (pp. 93-105). Springer, Dordrecht.

Leckie, D., Gougeon, F., Hill, D., Quinn, R., Armstrong, L. and Shreenan, R., 2003. Combined high-density lidar and multispectral imagery for individual tree crown analysis. *Canadian Journal of Remote Sensing*, *29*(5), pp.633-649.

Lehberger, M., Kleih, A.K. and Sparke, K., 2021. Self-reported well-being and the importance of green spaces–A comparison of garden owners and non-garden owners in times of COVID-19. *Landscape and Urban Planning*, *212*, p.104108.

Li, C., Yin, J. and Zhao, J., 2010, June. Extraction of urban vegetation from high-resolution remote sensing image. In *2010 International Conference On Computer Design and Applications* (Vol. 4, pp. V4-403). IEEE.

Li, M., Ma, L., Blaschke, T., Cheng, L. and Tiede, D., 2016. A systematic comparison of different object-based classification techniques using high spatial resolution imagery in agricultural environments. *International Journal of Applied Earth Observation and Geoinformation*, *49*, pp.87-98.

Liang, H.L., Li, W.Z., Zhang, Q.P., Zhu, W., Chen, D., Liu, J., Shu, T., 2017. Using unmanned aerial vehicle data to assess the three-dimension green quantity of urban green space: A case study in Shanghai, China. *Landscape Urban Plan* 164, 81-90.

Lim, S. and Lee, K.T., 2012. Implementation of biofuels in Malaysian transportation sector towards sustainable development: A case study of international cooperation between Malaysia and Japan. *Renewable and Sustainable Energy Reviews*, *16*(4), pp.1790-1800.

Liu, T. and Yang, X., 2013. Mapping vegetation in an urban area with stratified classification and multiple endmember spectral mixture analysis. *Remote Sensing of Environment*, *133*, pp.251-264.

Lloyd, R., Hodgson, M.E. and Stokes, A., 2002. Visual categorization with aerial photographs. *Annals of the Association of American Geographers*, *92*(2), pp.241-266.

Lõhmus, M. and Balbus, J., 2015. Making green infrastructure healthier infrastructure. *Infection ecology & epidemiology*, *5*(1), p.30082.

Lowe, S.H. and Guo, X., 2011. Detecting an optimal scale parameter in object-oriented classification. *IEEE Journal of Selected Topics in Applied Earth Observations and Remote Sensing*, *4*(4), pp.890-895.

Ma, L., Fu, T., Blaschke, T., Li, M., Tiede, D., Zhou, Z., Ma, X. and Chen, D., 2017a. Evaluation of feature selection methods for object-based land cover mapping of unmanned aerial vehicle imagery using random forest and support vector machine classifiers. *ISPRS International Journal of Geo-Information*, *6*(2), p.51.

Ma, L., Li, M., Ma, X., Cheng, L., Du, P. and Liu, Y., 2017b. A review of supervised object-based land-cover image classification. *ISPRS Journal of Photogrammetry and Remote Sensing*, *130*, pp.277-293.

Masson, V., Lemonsu, A., Hidalgo, J. and Voogt, J., 2020. Urban climates and climate change. *Annual Review of Environment and Resources*, *45*, pp.411-444.

Mathieu, R., Freeman, C. and Aryal, J., 2007. Mapping private gardens in urban areas using object-oriented techniques and very high-resolution satellite imagery. *Landscape and urban planning*, *81*(3), pp.179-192.

Möller, M., Lymburner, L. and Volk, M., 2007. The comparison index: A tool for assessing the accuracy of image segmentation. *International Journal of Applied Earth Observation and Geoinformation*, *9*(3), pp.311-321.

Moon, S.Y., Kim, J., Chong, W.K. and Ariaratnam, S.T., 2018. Urban green space layouts and urban heat island: Case study on apartment complexes in South Korea. *Journal of Urban Planning and Development*, *144*(2), p.04018004.

Mountrakis, G., Im, J. and Ogole, C., 2011. Support vector machines in remote sensing: A review. *ISPRS Journal of Photogrammetry and Remote Sensing*, *66*(3), pp.247-259.

Mukherjee, M. and Takara, K., 2018. Urban green space as a countermeasure to increasing urban risk and the UGS-3CC resilience framework. *International Journal of Disaster Risk Reduction*, *28*, pp.854-861.

Munyati, C., 2018. Optimising multiresolution segmentation: Delineating savannah vegetation boundaries in the Kruger National Park, South Africa, using Sentinel 2 MSI imagery. *International Journal of Remote Sensing*, *39*(18), pp.5997-6019.

Myint, S.W., Gober, P., Brazel, A., Grossman-Clarke, S. and Weng, Q., 2011. Per-pixel vs. object-based classification of urban land cover extraction using high spatial resolution imagery. *Remote sensing of environment*, 115(5), pp.1145-1161.

Newlone, R. 2022. Is there anything green about plastic grass?. *BBC News*. [Online]. 7 August. [Accessed: 4 September 2022]. Available from: https://www.bbc.co.uk/news/business-61552315

Nissar, A.K. and Nuzhat, S., 2016. Population growth, urban expansion and housing scenario in Srinagar City, J&K, India. *Journal of Geography and Regional planning*, 9(1), pp.1-11.

Nouri, H., Chavoshi Borujeni, S., Alaghmand, S., Anderson, S.J., Sutton, P.C., Parvazian, S. and Beecham, S., 2018. Soil salinity mapping of urban greenery using remote sensing and proximal sensing techniques; the case of Veale Gardens within the Adelaide Parklands. *Sustainability*, *10*(8), p.2826.

Nowak, D.J., Rowntree, R.A., McPherson, E.G., Sisinni, S.M., Kerkmann, E.R. and Stevens, J.C., 1996. Measuring and analyzing urban tree cover. *Landscape and Urban Planning*, *36*(1), pp.49-57.

Office for National Statistics, 2020. *One in eight British households has no garden*. [Online]. [Accessed: 11 July 2022]. Available from: https://www.ons.gov.uk/economy/environmentalaccounts/articles/oneineightbritishhouseholdshasnogarden/2020-05-14

OS GB National Grid Squares [Shape geospatial data], Scale 1:250 000, Tile(s): SU31NE, SU31SE, SU41NW, SU41SW, SU41NE, SU41SE, Updated: December 2012, Ordnance Survey, Using: EDINA Digimap Ordnance Survey Service. [Online]. [Accessed: 08 August 2022]. Available from: https://digimap.edina.ac.uk/os

OS MasterMap Greenspace Layer [Shape Geospatial Data], Scale 1:2500, Tile(s): SU31NE, SU31SE, SU41NW, SU41SW, SU41NE, SU41SE, Updated: October 2021, Ordnance Survey, Using: EDINA Digimap Ordnance Survey Service. [Online]. [Accessed: 22 July 2022]. Available from: https://digimap.edina.ac.uk/os

OS Open Greenspaces Map [Shape geospatial data], Scale 1:25 000, Tile(s): SU31NE, SU31SE, SU41NW, SU41SW, SU41NE, SU41SE, Updated: April 2022, Ordnance Survey, Using: EDINA Digimap Ordnance Survey Service. [Online]. [Accessed: 22 July 2022]. Available from: https://digimap.edina.ac.uk/os

Pal, N.R. and Pal, S.K., 1993. A review on image segmentation techniques. *Pattern recognition*, *26*(9), pp.1277-1294.

Parmehr, E.G., Amati, M., Taylor, E.J. and Livesley, S.J., 2016. Estimation of urban tree canopy cover using random point sampling and remote sensing methods. *Urban Forestry & Urban Greening*, *20*, pp.160-171.

Plaziak, M. and Szymanska, A.I., 2014. Construction sector in the Czech Republic and Poland: focus on the housing segment in selected regions. *Entrepreneurial Business and Economics Review*, *2*(2), p.47.

Powers, R.P., Hay, G.J. and Chen, G., 2012. How wetland type and area differ through scale: A GEOBIA case study in Alberta's Boreal Plains. *Remote Sensing of Environment*, *117*, pp.135-145

Pu, R. and Landry, S., 2012. A comparative analysis of high spatial resolution IKONOS and WorldView-2 imagery for mapping urban tree species. *Remote Sensing of Environment*, *124*, pp.516-533.

Ramirez, K.S., Leff, J.W., Barberán, A., Bates, S.T., Betley, J., Crowther, T.W., Kelly, E.F., Oldfield, E.E., Shaw, E.A., Steenbock, C. and Bradford, M.A., 2014. Biogeographic patterns in below-ground diversity in New York City's Central Park are similar to those observed globally. *Proceedings of the royal society B: biological sciences*, *281*(1795), p.20141988.

Ridgley, H., Hands, A., Lovell, R., Petrokofsky, C., Stimpson, A., Feeley, A., Bedford, A., Fenech, B., Leeman, D., Skykes, E. and Price, G., 2020. Improving access to green space A new review for 2020. *Public Health England*. [Online]. [Accessed: 9 July 2022]. Available from: https://assets.publishing.service.gov.uk/government/uploads/system/uploads/attachment_data/file/904439/Improving_access_to_green space_2020_review.pdf

Rosina, K. and Kopecká, M., 2016, June. Mapping of urban green spaces using Sentinel-2A data: Methodical aspects. In *6th International Conference on Cartography and GIS, Albena. Bulgarian Cartographic Association (in print)* (pp. 562-568).

Rouse Jr, J.W., Haas, R.H., Deering, D.W., Schell, J.A. and Harlan, J.C., 1974. *Monitoring the vernal advancement and retrogradation (green wave effect) of natural vegetation* (No. E75-10354).

Roy, S., Byrne, J. and Pickering, C., 2012. A systematic quantitative review of urban tree benefits, costs, and assessment methods across cities in different climatic zones. *Urban forestry & urban greening*, *11*(4), pp.351-363.

Rutzinger, M., Rottensteiner, F. and Pfeifer, N., 2009. A comparison of evaluation techniques for building extraction from airborne laser scanning. *IEEE Journal of selected topics in applied earth observations and remote sensing*, *2*(1), pp.11-20.

Salim, P.M., Ab Aziz, N.A., Khalid, N., Othman, A.N. and Salleh, S.A., 2018, October. Comparison of Segmentation Algorithm for Urban Tree Delineation using Aerial Imagery. In *2018 IEEE 8th International Conference on System Engineering and Technology (ICSET)* (pp. 139-143). IEEE.

Santamouris, M., 2018. *Minimizing energy consumption, energy poverty and global and local climate change in the built environment: innovating to zero: causalities and impacts in a zero concept world*. Elsevier.

Schumacher, P. and Duan, X., 2020. An Architecture for Cyborg Super-Society. In *Architectural Intelligence* (pp. 31-58). Springer, Singapore.

Semeraro, T., Scarano, A., Buccolieri, R., Santino, A. and Aarrevaara, E., 2021. Planning of urban green spaces: An ecological perspective on human benefits. *Land*, *10*(2), p.105.

Shackelford, A.K. and Davis, C.H., 2003. A combined fuzzy pixel-based and object-based approach for classification of high-resolution multispectral data over urban areas. *IEEE Transactions on GeoScience and Remote sensing*, *41*(10), pp.2354-2363.

Shackleton, S., Chinyimba, A., Hebinck, P., Shackleton, C. and Kaoma, H., 2015. Multiple benefits and values of trees in urban landscapes in two towns in northern South Africa. *Landscape and Urban Planning*, 136, pp.76-86.

Shahtahmassebi, A.R., Li, C., Fan, Y., Wu, Y., Gan, M., Wang, K., Malik, A. and Blackburn, G.A., 2021. Remote sensing of urban green spaces: A review. *Urban Forestry & Urban Greening*, *57*, p.126946.

Shanahan, D.F., Lin, B.B., Gaston, K.J., Bush, R. and Fuller, R.A., 2015. What is the role of trees and remnant vegetation in attracting people to urban parks?. *Landscape Ecology*, *30*(1), pp.153-165.

Shashua-Bar, L. and Hoffman, M.E., 2000. Vegetation as a climatic component in the design of an urban street: An empirical model for predicting the cooling effect of urban green areas with trees. *Energy and buildings*, *31*(3), pp.221-235.

Shekhar, S. and Aryal, J., 2019. Role of geospatial technology in understanding urban green space of Kalaburagi city for sustainable planning. *Urban Forestry & Urban Greening*, *46*, p.126450.

Shojanoori, R. and Shafri, H.Z., 2016. Review on the use of remote sensing for urban forest monitoring. *Arboric. Urban For*, *42*(6), pp.400-417.

Shortt, N.K., Rind, E., Pearce, J. and Mitchell, R., 2014. Integrating environmental justice and socioecological models of health to understand population-level physical activity. *Environment and Planning* A, 46(6), pp.1479-1495.

Silver, M., Tiwari, A. and Karnieli, A., 2019. Identifying vegetation in arid regions using object-based image analysis with RGB-only aerial imagery. *Remote Sensing*, *11*(19), p.2308.

Siregar, V.P., Prabowo, N.W., Agus, S.B. and Subarno, T., 2018, July. The effect of atmospheric correction on object based image classification using SPOT-7 imagery: a case study in the

Harapan and Kelapa Islands. In *IOP Conference Series: Earth and Environmental Science* (Vol. 176, No. 1, p. 012028). IOP Publishing.

Soga, M., Gaston, K.J. and Yamaura, Y., 2017. Gardening is beneficial for health: A meta-analysis. *Preventive medicine reports*, *5*, pp.92-99.

Song, C., Woodcock, C.E., Seto, K.C., Lenney, M.P. and Macomber, S.A., 2001. Classification and change detection using Landsat TM data: when and how to correct atmospheric effects?. *Remote sensing of Environment*, *75*(2), pp.230-244.

Southampton City Council 2020. Southampton City Council Green City Plan 2030: To Create a Cleaner, Greener, Healthier and More Sustainable City. Southampton City Council.

Spronken-Smith, R.A. and Oke, T.R., 1998. The thermal regime of urban parks in two cities with different summer climates. *International journal of remote sensing*, *19*(11), pp.2085-2104.

Stehman, S.V. and Wickham, J.D., 2011. Pixels, blocks of pixels, and polygons: Choosing a spatial unit for thematic accuracy assessment. *Remote Sensing of Environment*, *115*(12), pp.3044-3055.

Su, T. and Zhang, S., 2017. Local and global evaluation for remote sensing image segmentation. *ISPRS Journal of Photogrammetry and Remote Sensing*, *130*, pp.256-276.

Su, Y., Liu, L., Wu, J., Chen, X., Shang, J., Ciais, P., Zhou, G., Lafortezza, R., Wang, Y., Yuan, W. and Wang, Y., 2019. Quantifying the biophysical effects of forests on local air temperature using a novel three-layered land surface energy balance model. *Environment international*, *132*, p.105080.

Sun, Z. and Meng, Q., 2020. Object-based automatic multi-index built-up areas extraction method for WorldView-2 satellite imagery. *Geocarto international*, *35*(8), pp.801-817.

Sung, C.Y., 2012. Evaluating the efficacy of a local tree protection policy using LiDAR remote sensing data. *Landscape and Urban Planning*, 104(1), pp.19-25.

Szilassi, P., Breuste, J., Kolcsár, R.A. and Aigner, G., 2020. Mobile Application-based Field Survey as a Possible Tool for Investigating Visitors' Perception and Preferences of the Vegetation in Urban Parks.

Tan, M., Li, X., Xie, H. and Lu, C., 2005. Urban land expansion and arable land loss in China—a case study of Beijing–Tianjin–Hebei region. *Land use policy*, *22*(3), pp.187-196.

Tanhuanpää, T., Vastaranta, M., Kankare, V., Holopainen, M., Hyyppä, J., Hyyppä, H., Alho, P. and Raisio, J., 2014. Mapping of urban roadside trees–A case study in the tree register update process in Helsinki City. *Urban forestry & urban greening*, *13*(3), pp.562-570.

Taubenböck, H., Felbier, A., Esch, T., Roth, A. and Dech, S., 2012. Pixel-based classification algorithm for mapping urban footprints from radar data: a case study for RADARSAT-2. *Canadian Journal of Remote Sensing*, *38*(3), pp.211-222.

Taylor, L. and Hochuli, D.F., 2017. Defining green space: Multiple uses across multiple disciplines. *Landscape and urban planning*, *158*, pp.25-38.

Theodorou, A., Panno, A., Carrus, G., Carbone, G.A., Massullo, C. and Imperatori, C., 2021. Stay home, stay safe, stay green: The role of gardening activities on mental health during the Covid-19 home confinement. *Urban Forestry & Urban Greening*, *61*, p.127091.

ThiLoi, D., Tuan, P.A. and Gupta, K., 2015. Development of an index for assessment of urban green spacesat city level. *International Journal of Remote Sensing Applications*, *5*(1), p.78.

Thurnhofer, S. and Mitra, S.K., 1996. Edge-enhanced image zooming. *Optical Engineering*, *35*(7), pp.1862-1870.

Tigges, J., Lakes, T. and Hostert, P., 2013. Urban vegetation classification: Benefits of multitemporal RapidEye satellite data. *Remote Sensing of Environment*, *136*, pp.66-75.

Toutin, T., 2004. Geometric processing of remote sensing images: models, algorithms and methods. *International journal of remote sensing*, *25*(10), pp.1893-1924.

Tullis, J.A. and Jensen, J.R., 2003. Expert system house detection in high spatial resolution imagery using size, shape, and context. *Geocarto International*, *18*(1), pp.5-15.

Twohig-Bennett, C. and Jones, A., 2018. The health benefits of the great outdoors: A systematic review and meta-analysis of green space exposure and health outcomes. *Environmental research*, *166*, pp.628-637.

United Nations, 2015. *Sustainable development goals, Goal 11.* [Online]. [Accessed: 7 August 2022]. Available from: http://www.ueha.co.uk/uploads/2/5/6/4/25647797/ueha__conservation_guidelines__aug_2020.pdf

United Nations, 2019. World Urbanization Prospects: The 2018 Revision. In *Department of Economic and Social Affairs Population Division ST/ESA/SER.A/420*. [Online]. [Accessed: 22 August 2022]. Available from: https://population.un.org/wup/Publications/Files/WUP2018-Report.pdf.

Van de Voorde, T., 2017. Spatially explicit urban green indicators for characterizing vegetation cover and public green space proximity: A case study on Brussels, Belgium. *International Journal of Digital Earth*, *10*(8), pp.798-813.

Vigneshwaran, S. and Vasantha Kumar, S., 2021. Comparison of classification methods for urban green space extraction using very high-resolution worldview-3 imagery. *Geocarto International*, *36*(13), pp.1429-1442.

Walsh, K.B., Blasco, J., Zude-Sasse, M. and Sun, X., 2020. Visible-NIR 'point'spectroscopy in postharvest fruit and vegetable assessment: The science behind three decades of commercial use. *Postharvest Biology and Technology*, *168*, p.111246.

Wang, X., Qu, K., Xu, B., Ren, J. and Qu, X., 2011. Microwave assisted one-step green synthesis of cell-permeable multicolor photoluminescent carbon dots without surface passivation reagents. *Journal of Materials Chemistry*, *21*(8), pp.2445-2450.

Wei, W., Chen, X. and Ma, A., 2005, July. Object-oriented information extraction and application in high-resolution remote sensing image. In *Proceedings. 2005 IEEE International Geoscience and Remote Sensing Symposium, 2005. IGARSS'05.* (Vol. 6, pp. 3803-3806). Ieee.

Weng, Q., 2012. *An introduction to contemporary remote sensing*. McGraw-Hill Education.

Whiteside, T.G., Boggs, G.S. and Maier, S.W., 2011. Comparing object-based and pixel-based classifications for mapping savannas. *International Journal of Applied Earth Observation and Geoinformation*, *13*(6), pp.884-893.

Wilby, R.L., 2003. Past and projected trends in London's urban heat island. *Weather*, *58*(7), pp.251-260.

Witharana, C. and Civco, D.L., 2014. Optimizing multi-resolution segmentation scale using empirical methods: Exploring the sensitivity of the supervised discrepancy measure Euclidean distance 2 (ED2). *ISPRS Journal of Photogrammetry and Remote Sensing*, *87*, pp.108-121.

Wood, E.M. and Esaian, S., 2020. The importance of street trees to urban avifauna. *Ecological Applications*, *30*(7), p.e02149.

World Health Organization, 2016. Urban green spaces and health (No. WHO/EURO: 2016-3352-43111-60341). Copenhagen: World Health Organization. Regional Office for Europe.

Xu, H., 2013. Rule-based impervious surface mapping using high spatial resolution imagery. Int. J. Remote Sens. 34 (1), 27–44.

Xu, H., Ding, F. and Wen, X., 2009. Urban expansion and heat island dynamics in the Quanzhou region, China. *IEEE Journal of selected topics in applied earth observations and remote sensing*, *2*(2), pp.74-79.

Yang, Y., Wang, J., Chen, Y., Cheng, F., Liu, G. and He, Z., 2019. Remote-sensing monitoring of grassland degradation based on the GDI in Shangri-La, China. *Remote Sensing*, *11*(24), p.3030.

Yu, Z., Wang, Y., Deng, J., Shen, Z., Wang, K., Zhu, J. and Gan, M., 2017. Dynamics of hierarchical urban green space patches and implications for management policy. *Sensors*, *17*(6), p.1304.

Zhang, B., Xie, G., Zhang, C. and Zhang, J., 2012. The economic benefits of rainwater-runoff reduction by urban green spaces: A case study in Beijing, China. *Journal of environmental management*, 100, pp.65-71.

Zhao, P., Lü, B. and de Roo, G., 2010. Urban expansion and transportation: The impact of urban form on commuting patterns on the city fringe of Beijing. *Environment and Planning A*, *42*(10), pp.2467-2486.

Zhen, Z., Quackenbush, L.J. and Zhang, L., 2016. Trends in automatic individual tree crown detection and delineation—Evolution of LiDAR data. *Remote Sensing*, *8*(4), p.333.

Zou, H. and Wang, X., 2021. Progress and gaps in research on urban green space morphology: A review. *Sustainability*, *13*(3), p.1202.

APPENDICES

Appendix 1 Estimated Scale Parameters and Numbers of Objects of the 0.2 m resolution data (Figure 3.4) as Level 1 and 3.

Level 1

Shape (0.1 – 0.9)	**Compactness (0.1 – 0.9)**	**Scale Parameter**	**Number of Objects**
0.1	0.1	73	118
0.1	0.5	28	549
0.1	0.9	73	123
0.5	0.1	54	153
0.5	0.5	48	195
0.5	0.9	58	147
0.9	0.1	37	141
0.9	0.5	36	167
0.9	0.9	31	267

Level 3

Shape (0.1 – 0.9)	**Compactness (0.1 – 0.9)**	**Scale Parameter**	**Number of Objects**
0.1	0.1	713	1
0.1	0.5	628	1
0.1	0.9	623	1
0.5	0.1	474	1
0.5	0.5	338	1
0.5	0.9	338	1
0.9	0.1	187	1
0.9	0.5	176	1
0.9	0.9	161	1

Appendix 2 Estimated Scale Parameters and Numbers of Objects of the 1 m resolution data (Figure 3.5) as Level 1 and 2.

Level 1

Compactness (0.1 – 0.9)	Shape (0.1 – 0.9)	Scale Parameter	Number of Objects
0.1	0.1	136	758
0.1	0.5	102	774
0.1	0.9	44	978
0.5	0.1	137	754
0.5	0.5	96	865
0.5	0.9	52	727
0.9	0.1	146	672
0.9	0.5	104	778
0.9	0.9	61	574

Level 2

Compactness (0.1 – 0.9)	Shape (0.1 – 0.9)	Scale Parameter	Number of Objects
0.1	0.1	226	271
0.1	0.5	212	214
0.1	0.9	104	199
0.5	0.1	197	394
0.5	0.5	226	177
0.5	0.9	102	212
0.9	0.1	276	209
0.9	0.5	224	187
0.9	0.9	91	269

Appendix 3 Confusion matrix of Supervised Classification the Study Area

		Reference Data								
	Class	Grassland	Industrial Area	Residential Area	Roads	Trees	Water		**TOTAL**	**User Accuracy(%)**
Classification	Grassland	7	1	0	1	0	1		10	70
	Industrial Area	3	12	1	3	1	0		20	60
	Residential Area	0	0	10	2	0	1		13	76.9
	Roads	1	1	3	9	0	2		14	64.3
	Trees	5	0	0	1	15	0		21	71.4
	Water	2	1	3	2	0	14		22	63.6
	TOTAL	18	15	17	18	16	16		100	
	Producer Accuracy(%)	38.9	80	58.9	50	93.8	87.5		**Overall Accuracy**	67
									Kappa	0.61

Appendix 4 Confusion matrix of Ruleset 1 the Test Area Vertical Aerial Photography

Reference Data										
Classified Image	Class	Construction Site	Grassland	Non-residential	Residential	Roads	Trees	Water	**TOTAL**	User Accuracy (%)
	Construction Site	4				1			5	80
	Grassland		18				2	1	21	85.71
	Non-residential			12	2	1			15	80
	Residential			1	1				2	50
	Roads	2	3	1		21		4	31	67.74
	Trees		3				5		8	62.50
	Water	1		2		1		14	18	77.78
	TOTAL	7	24	16	3	24	7	19	100	
	Producer Accuracy (%)	57.14	75	75	33.33	87.50	71.42	73.68		Overall:75% Kappa: 0.69

Appendix 5 Confusion matrix of Ruleset 2 the Test Area CASI

		Reference Data									
	Class	Grassland	Non-residential	Residential	Roads	Trees	Water		**TOTAL**	**User Accuracy (%)**	
Classification	Grassland	9	2		1	1	5		18	50	
	Non-residential		1		1				2	50	
	Residential		2	0	3				5	0.00	
	Roads		1		5				6	83	
	Trees	11	1	14	10	10	1		47	21	
	Water	1	4		2		15		22	68	
	TOTAL	21	11	14	22	11	21	100	100		
										Overall Accuracy	40 %
	Producer Accuracy(%)	43	9	0.00	23	91	71			**Kappa**	0.29

Appendix 6 Confusion matrix of Ruleset 2 the Test Area Vertical Aerial Photography

		Reference Data								
	Class	Grassland	Non-residential	Residential	Roads	Trees	Water		**TOTAL**	**User Accuracy(%)**
Classification	Grassland	14	0	0	1	2	0		17	82
	Non-residential	0	12	2	0	0	0		14	86
	Residential	1	3	6	0	0	1		11	55
	Roads	0	3	0	26	0	2		31	84
	Trees	1	0	0	1	10	0		12	83
	Water	1	0	0	0	0	14		15	93
	TOTAL	17	18	8	28	12	17		100	
	Producer Accuracy(%)	82	67	75	93	83	82		**Overall Accuracy**	82
									Kappa	0.78

Appendix 7 Confusion matrix of Ruleset 2 the Study Area Object-based Classification

		Reference Data								
Classification	**Class**	Grassland	Non-residential	Residential	Roads	Trees	Water	**TOTAL**		User Accuracy(%)
	Grassland	19			3	3	2	27		70
	Non-residential		11		2		3	16		69
	Residential			7	4			11		64
	Roads		1	2	11		1	15		73
	Trees	3	1			9		13		69
	Water	1			2		15	18		83
	TOTAL	23	13	9	22	12	21	100		
	Producer Accuracy (%)	83	85	78	50	75	71		**Overall Accuracy**	72%
									Kappa	0.66